CYTOKINES

IL-2 is inactivated by the acidic pH environment of tumors enabling engineering of a pH-selective mutein

Silvia Gaggero[1]†, Jonathan Martinez-Fabregas[2]†‡, Adeline Cozzani[1], Paul K. Fyfe[2], Malo Leprohon[1,3], Jie Yang[4], F. Emil Thomasen[5], Hauke Winkelmann[6], Romain Magnez[1], Alberto G. Conti[4], Stephan Wilmes[2], Elizabeth Pohler[2], Manuel van Gijsel Bonnello[2], Xavier Thuru[1], Bruno Quesnel[1], Fabrice Soncin[7,8], Jacob Piehler[6], Kresten Lindorff-Larsen[5], Rahul Roychoudhuri[4]*§, Ignacio Moraga[2]*§, Suman Mitra[1]*§

Cytokines interact with their receptors in the extracellular space to control immune responses. How the physicochemical properties of the extracellular space influence cytokine signaling is incompletely elucidated. Here, we show that the activity of interleukin-2 (IL-2), a cytokine critical to T cell immunity, is profoundly affected by pH, limiting IL-2 signaling within the acidic environment of tumors. Generation of lactic acid by tumors limits STAT5 activation, effector differentiation, and antitumor immunity by CD8^{+} T cells and renders high-dose IL-2 therapy poorly effective. Directed evolution enabled selection of a pH-selective IL-2 mutein (Switch-2). Switch-2 binds the IL-2 receptor subunit IL-2Rα with higher affinity, triggers STAT5 activation, and drives CD8^{+} T cell effector function more potently at acidic pH than at neutral pH. Consequently, high-dose Switch-2 therapy induces potent immune activation and tumor rejection with reduced on-target toxicity in normal tissues. Last, we show that sensitivity to pH is a generalizable property of a diverse range of cytokines with broad relevance to immunity and immunotherapy in healthy and diseased tissues.

INTRODUCTION

Cytokines are small, secreted proteins that control all aspects of the immune response (1, 2). Despite their potential to treat cancer, few cytokines have reached the clinic due to limited efficacy and severe systemic toxicities (3), emphasizing the urgent need for more specific and less toxic cytokine-based therapies. Cytokines do not only activate signaling via receptor dimerization, triggering activation of the JAK (Janus kinase)/STAT (signal transducer and activator of transcription) signaling pathway but also can control the activity of diverse serine/threonine kinase signaling networks (4, 5). Interleukin-2 (IL-2) is a powerful regulator of immunity (6). High-dose IL-2 therapy is approved for the treatment of metastatic renal cell carcinoma and metastatic melanoma, but partial efficacy and high levels of systemic on-target toxicity have hindered its wider use (7). IL-2 binds a surface receptor composed of IL-2Rα, IL-2Rβ, and γc chains, triggering the activation of the JAK1/JAK3/STAT5 signaling

pathway (8, 9). In addition to STAT5, IL-2 engages non-STAT pathways that contribute to shaping its immunomodulatory properties (8).

Cancers develop mechanisms to evade and escape the immune response; key among them is the establishment of an immunosuppressive microenvironment (10). A hallmark of the tumor microenvironment (TME) is acidosis. Production of lactic acid by tumor cells results in an acidic environment of pH ~6.2 to 6.5, contrasting with pH ~7.4 found in normal tissues (11–13). The physicochemical environment of tumors profoundly shapes tumor immune responses. It inhibits the proliferation and cytotoxic activities of CD8 T and natural killer (NK) cells (14, 15) and the differentiation of monocytes into dendritic cells, thus affecting antitumor T cell responses (16). However, mechanisms by which it does so are incompletely elucidated. Given that cytokines interact with their receptors in the extracellular space, we asked whether the acidic extracellular environment of tumors compromises the activity of IL-2 within tumors.

[1]Inserm UMR1277, CNRS UMR9020-CANTHER, Université de Lille, Lille University Hospital, Lille, France. [2]Division of Cell Signaling and Immunology, School of Life Sciences, University of Dundee, Dundee, UK. [3]Université de Lille, CNRS, Inserm, CHU Lille, Institut Pasteur de Lille, US 41 - UAR 2014 - PLBS, F-59000 Lille, France. [4]Department of Pathology, University of Cambridge, Tennis Court Road, Cambridge, UK. [5]Structural Biology and NMR Laboratory, Linderstrøm-Lang Centre for Protein Science, Department of Biology, University of Copenhagen, DK-2200 Copenhagen, Denmark. [6]Department of Biology/Chemistry and Center for Cellular Nanoanalytics (CellNanOs), Osnabrück University, Barbarastr. 11, 49076 Osnabrück, Germany. [7]CNRS/IIS/Centre Oscar Lambret/Lille University SMMiL-E Project, CNRS Délégation Hauts-de-France, Lille, France. [8]CNRS IRL 2820; Laboratory for Integrated Micro Mechatronic Systems, Institute of Industrial Science, University of Tokyo, Tokyo, Japan.
†These authors contributed equally to this work.
‡Present address: Instituto de Investigaciones Químicas (IIQ), Centro de Investigaciones Científicas Isla de la Cartuja (cicCartuja), Universidad de Sevilla, CSIC, Sevilla, Spain.
§ These authors contributed equally to this work.
*Corresponding author. Email: suman.mitra@inserm.fr (S.M.); i.moragagonzalez@dundee.ac.uk (I.M.); rr257@cam.ac.uk (R.R.)

RESULTS

Acidic extracellular environment disrupts IL-2 signaling

We first asked whether acidic pH, similar to that found within the TME, alters IL-2 signaling and activity. We found that IL-2–driven STAT5 phosphorylation within preactivated CD8^{+} T cells was substantially reduced when cells were cultured in medium acidified to pH 6.5 (reflecting the pH found within tumors) from pH 7.5 through addition of HCl (Fig. 1A and fig. S1, A and B). IL-2 appears to be a weak agonist at acidic pH, with the amplitude of STAT5 phosphorylation, rather than the potency [median effective concentration (EC$_{50}$)], being affected. Similar results were found when the medium was acidified through addition of lactic acid but not through addition of NaCl (Fig. 1B). pH sensitivity was

Fig. 1. Low pH impairs IL-2 activity. (**A**) Dose-response of STAT5 phosphorylation in preactivated CD8^{+} T cells stimulated with IL-2 in medium at pH 7.5 or 6.5. (**B**) Dose-response of STAT5 phosphorylation in preactivated CD8^{+} T cells stimulated with IL-2 in medium at pH 7.5 ± 12 mM NaCl or in medium at pH 6.5 generated by addition of 12 mM HCl or 15 mM lactic acid (LA). Data are the pooled results of three independent experiments with technical duplicates. (**C**) Schema showing staining of IL-2–expressing yeast with bi-otinylated IL-2Rα and AF647-conjugated SA (left). Dose-dependent binding at different pH levels of IL-2Rα serial dilu-tions to the surface of IL-2–expressing yeast (right). (**D**) Effects of IL-2 treatment on tumor growth of B16.SIY tumors with or without NaHCO₃ treatment (*n* = 12 for each group). (**E**) Growth and survival curves of B16 WT or LDH KO tumors (*n* = 12 for each group). (**F** and **G**) STAT5 phosphorylation in CD8^{+} T cells from blood (F) and tumor (G). Representative histogram plots (left) of STAT5 phosphor-ylation and scatter plots (right) of the mean (*n* = 6 for each group). (**H** to **K**) Dot plots of representative samples (H and J) and percentages (I and K) showing the expression of IFN-γ and TNF (H and I) and PD-1 and TIM3 (J and K) in CD8^{+} T cells. Each symbol represents a single mouse (F, G, and K) (*n* = 18) or two mice pooled to-gether (I) (*n* = 9). Data are the pooled results of two (D to G) or three indepen-dent experiments (C, I, and K). Statistical significance was determined by one-way ANOVA with Tukey's correction [D, E (left), F, G, I, and K] or by the log-rank test with Bonferroni's correction (E, right).
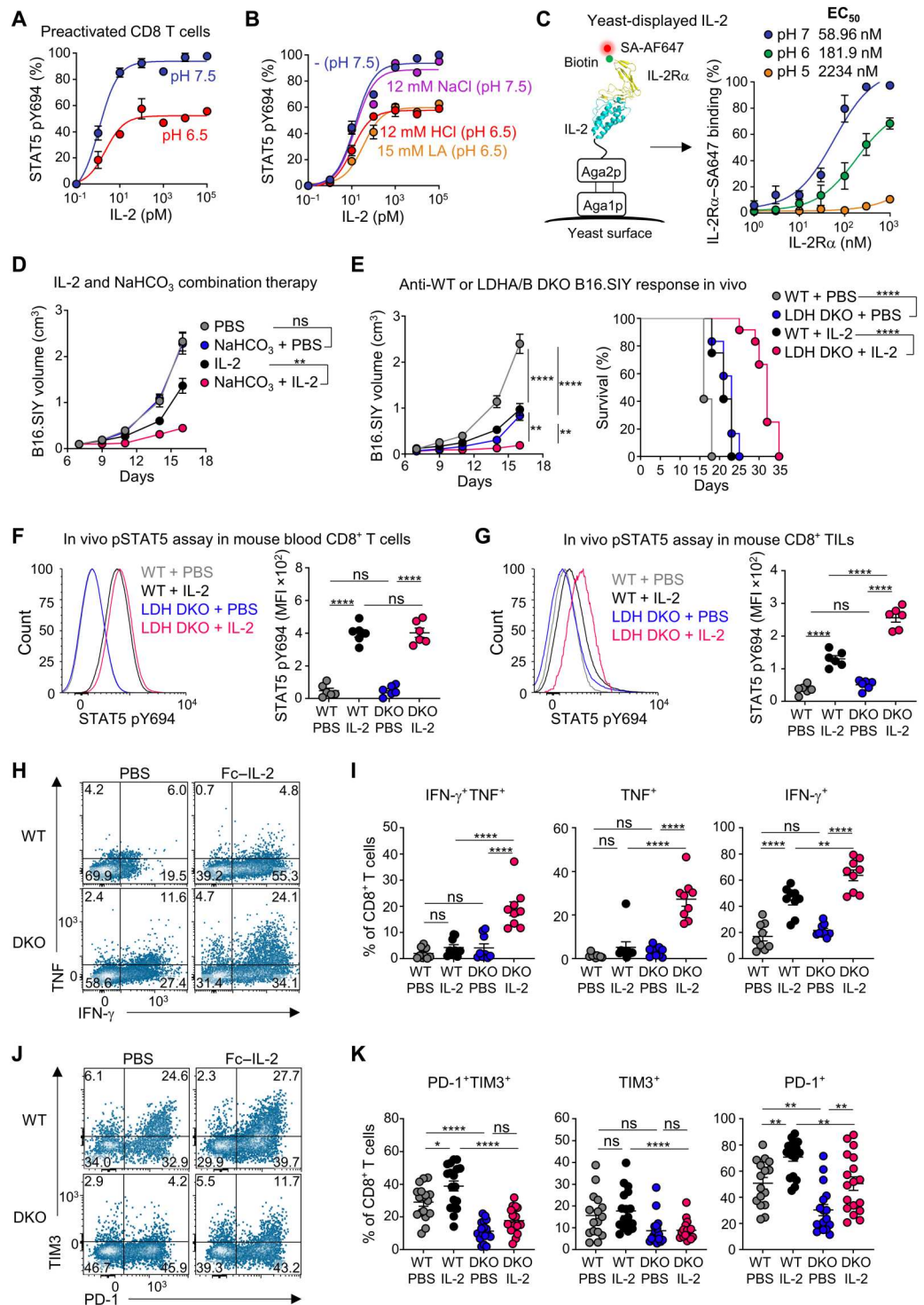
not unique to IL-2, with many other cytokines also exhibiting pH dependency (fig. S1, C and D). These preliminary data suggest that the activity of several cytokines might be regulated by the pH of the extracellular environment in which they operate.

We observed that IL-2 activated STAT5 to the same extent at pH 6.5 and 7.5 in resting IL-2Rα–negative CD8^{+} T cells, in contrast to IL-2Rα–positive preactivated CD8^{+} T cells, suggesting that acidic pH interferes with the binding of IL-2 to IL-2Rα (fig. S1E). To test this hypothesis, we took advantage of previously characterized IL-2Rα^{+} and IL-2Rα^{−} YT cell lines (*17*). Similar to preactivated CD8^{+} T cells, IL-2–driven signaling in IL-2Rα^{+} YT cells, but not in IL-2Rα^{−} YT cells, was diminished under acidic pH (fig. S1F), confirming that binding of IL-2 to IL-2Rα is pH dependent. More-over, using IL-2 surface-displayed on yeast, and microscale

thermophoresis (MST), we confirmed that IL-2:IL-2Rα binding is severely reduced at pH 6 or lower (Fig. 1C and fig. S1G). IL-2 binding to IL-2Rβ was only weakly affected by changes in acidic pH (fig. S1H), indicating that this is a specific effect affecting the IL-2:IL-2Rα interaction.

IL-2 antitumor activity is blocked by the acidic TME

We next investigated whether the acidic pH found in the TME negatively affects IL-2 therapy. We administered bicarbonate in vivo to neutralize the acidic pH of the TME (6). Combining bicarbonate treatment with IL-2 [IL-2 conjugated to the Fc portion of human immunoglobulin G4 (IgG4) (Fc-IL-2) to extend the half-life of IL-2 in vivo] improved antitumor responses in the B16.SIY melanoma model (Fig. 1D and fig. S2, A to C). Because lactic acid released by tumors is one of the major contributors to the acidic TME, we used previously described B16.SIY melanoma cells lacking expression of lactate dehydrogenase A and B (LDHA/B) to further assess the effect of intratumoral acidosis on IL-2 therapy (13). Mice were injected with wild-type (WT) B16.SIY cells or with LDHA/B double-knockout (LDHA/B DKO) B16.SIY cells and treated with IL-2 (fig. S2D). Fc-IL-2 therapy minimally reduced tumor growth and increased survival in mice bearing B16.SIY WT tumors (Fig. 1E and fig. S2E). However, in mice bearing LDHA/B DKO B16.SIY tumors, Fc-IL-2 therapy significantly reduced tumor growth and increased survival (Fig. 1D and fig. S2E), again suggesting that tumor acidosis impairs the efficacy of IL-2 therapy.

We evaluated IL-2 activity in CD8+ T cells from WT and LDH DKO B16.SIY tumor–bearing mice by directly measuring pSTAT5 levels via flow cytometry in blood versus tumor-infiltrating CD8+ T lymphocytes upon IL-2 administration. Whereas no difference was observed in the levels of IL-2–induced STAT5 phosphorylation in blood CD8+ T cells (Fig. 1F), STAT5 signaling was significantly reduced in tumor-infiltrating CD8+ T cells within WT tumors compared with LDH DKO tumors (Fig. 1G), demonstrating that IL-2 signaling is diminished by the acidotic environment of tumors. Fc-IL-2 treatment did not significantly increase the number of CD8+ T tumor-infiltrating lymphocytes (TILs) or the ratio of CD8+ T cells to regulatory T (Treg) cells in LDHA/B DKO B16.SIY as compared with B16.SIY tumors (fig. S2, F to I). However, in LDHA/B DKO B16.SIY tumors, Fc-IL-2 treatment markedly increased the capacity of CD8 TIL to produce interferon-γ (IFN-γ) and tumor necrosis factor (TNF) (Fig. 1, H and I) and reduced the frequency of exhausted CD8+ T cells (Fig. 1, J and K). These findings show that the acidic pH found within tumors inhibits IL-2–driven immunotherapy responses.

## Engineering of a pH-selective IL-2 mutein

Given that IL-2 is unable to function at acidic extracellular pH, we used directed evolution to identify IL-2 mutants with improved binding to IL-2Rα at low pH. We created mutant libraries of IL-2 by introducing mutations to the 13–amino acid residues at its interface with IL-2Rα (Fig. 2A and fig. S3, A and B) using degenerate "NDT" codons encoding for Gly, Val, Leu, Ile, Cys, Ser, Arg, His, Asp, Asn, Phe, and Tyr amino acids. The mutant library was displayed on the surface of yeast by fusion to the yeast protein Aga2p (Fig. 2A). In vitro directed evolution was performed by sequential enrichment of yeast binding to decreasing concentrations of the IL-2Rα ectodomain at pH 5 (Fig. 2A), leading to the identification of an IL-2 variant, hereinafter named Switch-2,

characterized by Thr[37]His, Arg[38]Leu, Thr[41]Ser, Phe[42]Tyr, and Lys[43]Gly mutations (fig. S3, A and B). We found that Switch-2 not only displayed higher binding to IL-2Rα at low pH but also that its behavior was pH selective, reflected in lower binding at neutral pH as compared with WT IL-2 (Fig. 2B and fig. S3C). Mutations in Switch-2 did not alter its affinity toward IL-2Rβ at neutral and acidic pH compared with IL-2 (figs. S1H and S3D). Next, we assessed the ability of IL-2 and Switch-2 to interact with IL-2Rα on the membranes of living cells at neutral versus acidic pH using single-molecule total internal fluorescence (TIRF) microscopy (Fig. 2C). For this purpose, IL-2Rα fused to an N-terminal SNAPf-tag was stably expressed in HeLa cells and substoichiometrically labeled with SNAP-Surface 547 to ensure robust quantification by single-molecule localization. After adding DY647-labeled IL-2 and Switch-2, respectively, we measured IL-2Rα and IL-2 densities in individual cells by dual-color single-molecule localization microscopy to quantify relative binding levels at different pH conditions (Fig. 2, C and D, and movies S1 to S4). These experiments showed substantially reduced IL-2 binding to IL-2Rα at pH 6 as compared with neutral pH. By contrast, Switch-2 showed an opposing relationship, exhibiting a strong ligand-receptor interaction at acidic pH and minimal interaction at neutral pH, again confirming its pH-selective binding to IL-2Rα (Fig. 2D). Analysis of thermal unfolding profiles revealed that IL-2 and Switch-2 exhibited comparable thermal stability not affected by low pH (fig. S3E), indicating that low pH specifically inhibits IL-2 signaling by hindering cytokine-receptor interaction and not by reducing protein stability in the cellular context.

To determine the structural basis by which Switch-2 exhibits pH-dependent receptor binding, we solved the structure of the Switch-2:IL-2Rα complex to 3.2 Å resolution (Fig. 2E). Superposition of the complexes formed by Switch-2 and WT IL-2 showed no major perturbations in their receptor binding architecture, with a root mean square deviation (RMSD) of 1.56 Å. At the Switch-2:IL-2Rα binding interface, side-chain densities were clear for the amino acid mutations found in Switch-2 (fig. S4A). Despite overall similarity in the topology of binding between the IL-2 and Switch-2 complexes, the electrostatic interaction networks of the two structures differed significantly in the mutated region (Fig. 2, E and F). In the IL-2:IL-2Rα structure, an extensive network was observed. Interchain salt bridges are located at either end of this region, formed by Glu[29]:Lys[43] and Asp[6]:Arg[38] of IL-2Rα and IL-2, respectively (Fig. 2F). The side chain of Arg[38] is positioned such that it may form a further hydrogen bond to His[120] of IL-2Rα, which itself can also form a second hydrogen bond to Asn[27] of IL-2Rα (Fig. 2F). Much of this network is lost in Switch-2, replaced with just a single interchain hydrogen bond between Tyr[42] of Switch-2 and Asn[27] of IL-2Rα (Fig. 2F).

A close examination of the IL-2–IL-2Rα binding interface reveals a putative "pH Switch" consisting of the interaction between Arg[38] in IL-2 and His[120] in IL-2Rα (Fig. 2F). We hypothesized that, at the low pH in the TME, His[120] would become protonated, resulting in release of IL-2 from IL-2Rα and therefore lack of signaling. To test this hypothesis, we ran molecular dynamics simulations of the IL-2–IL-2Rα complex and Switch-2–IL-2Rα complex with histidine side chains protonated (corresponding to pH 6) or neutral (mimicking pH 7) and examined the structural stability of the complexes (fig. S4B). For IL-2–L-2Rα at pH 6, the complex fully dissociated within 4 μs in two of five replica simulations, whereas the
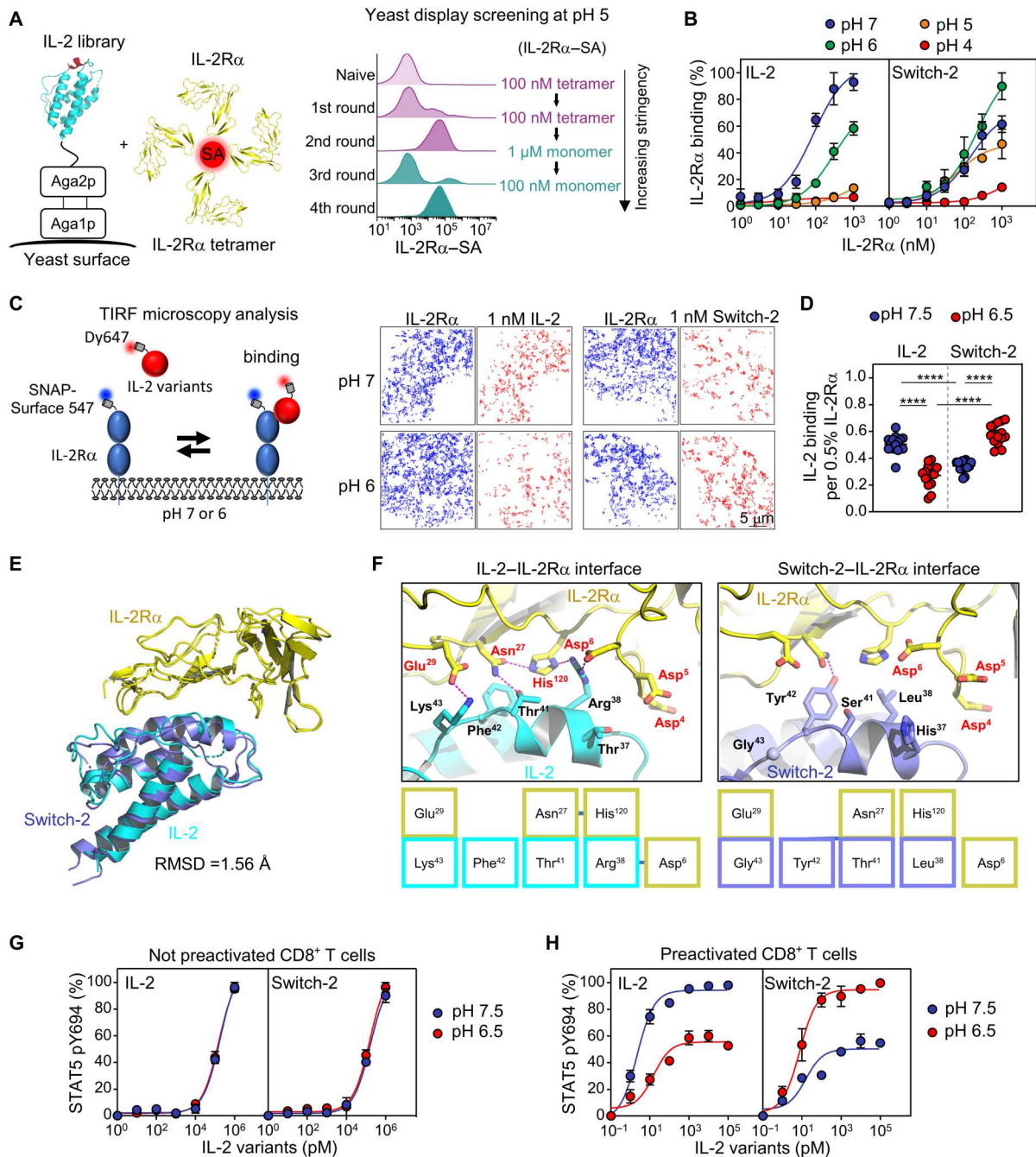
Fig. 2. Selection of a pH-resistant IL-2 variant. (**A**) Schematic representation of the IL-2 mutant library expressed at the yeast surface and interacting with the biotinylated IL-2Rα tetramer (left). Amino acids that were mutated during the generation of the IL-2 library are displayed in red. Histogram overlays assessing IL-2Rα staining of the library at each round of selection at pH 5 are shown (right). (**B**) Dose-dependent binding at different pH levels of IL-2Rα serial dilutions to IL-2 or Switch-2 displaying yeasts. (**C**) Quantification of the IL-2/IL-2Rα interaction at the plasma membrane of live cell by dual-color TIRF microscopy with labeled IL-2Rα and IL-2 (left) and representative images showing trajectories from 100 consecutive frames of simultaneous dual-color imaging of IL-2 and Switch-2 binding to IL-2Rα–expressing HeLa at different pH levels. (**D**) Graph showing the IL-2 binding normalized to the IL-2Rα cell surface expression. Each data point represents the result from a single cell. Significance was calculated by the Kolmogorov-Smirnov test. (**E**) Overlay of the IL-2:IL-2Rα and Switch-2:IL-2Rα complex crystal structures. IL-2 and Switch-2 engage IL-2Rα with identical geometry (RMSD = 1.56 Å). RMSD represents alignment of all atoms. Superposition of the C-alpha positions of the complexes formed by Switch-2 or WT IL-2 (PDB entry 1Z92), along with their partner CD25, with an RMSD of 1.53 Å² over 235 residues. IL-2 is colored in cyan, and Switch-2 is colored in slate blue. IL-2Rα is colored in yellow for the IL-2 and Switch-2 complexes. (**F**) Close-up views of the IL-2:IL-2Rα (left) and Switch-2:IL-2Rα (right) binding interfaces. Hydrogen bonds and salt bridges are shown as purple dashed lines. Hydrogen bonds were defined using standard accepted values of ~2.5 to 3.5 Å, with salt bridge lengths extending to 4.5 Å. Under each inset box, a 2D interaction map of the IL-2:IL-2Rα or Switch-2:IL-2Rα interface is shown. Amino acids are depicted as nodes in the interaction maps. Interactions between amino acids are shown as solid blue lines. (**G** and **H**) Dose-response curve of phospho-STAT5 induced by IL-2 and Switch-2 at pH 7.5 and 6.5 in not preactivated (G) and preactivated CD8 T cells (H). Data are the pooled results of two (B) or three independent experiments (G and H).

complex did not dissociate within 4 μs in any of the five replicas at pH 7, suggesting that the lowered stability of IL-2–IL-2Rα at acidic pH is due to protonation of histidines. In line with this, in the simulations that show dissociation, Arg[38] and His[120] were separated before the interaction interface is fully disrupted (fig. S4C and movie S5). For Switch-2–IL-2Rα, the complex did not dissociate within 4 μs in any of the five replicas at pH 6 or 7, suggesting that the decreased pH sensitivity of Switch-2 is due to loss of the Arg[38]-His[120] interaction. To ensure that dissociation was not the result of protein unfolding caused by high temperature in the simulations, we calculated the backbone RMSD over time for IL-2 and the IL-2 binding domain of IL-2Rα, and we observed in both cases that there was no substantial unfolding (fig. S5). Switch-2 has a histidine substitution at position 37, which is near Asp[4] and Asp[5] in IL-2Rα (Fig. 2F). It is thus tempting to speculate that Switch-2 presents a distinct pH Switch centered around His[37], which reinforces the stability of the Switch-2:IL-2Rα interface under acidic conditions.

Next, we investigated Switch-2 functionality at acidic pH. First, we characterized the levels of STAT5 phosphorylation induced by IL-2 and Switch-2 in non-preactivated and preactivated CD8^{+} T cells at pH 7.5 and 6.5. In resting IL-2Rα−negative CD8^{+} T cells, both IL-2 and Switch-2 induced comparable STAT5 activation at pH 6.5 and 7.5 (Fig. 2G). In preactivated CD8^{+} T cells, however, IL-2 triggered stronger STAT5 activation at pH 7.5 than at pH 6.5 (Fig. 2H). Switch-2, on the other hand, exhibited opposing behavior, triggering more potent STAT5 activation at pH 6.5 than at pH 7.5 (Fig. 2H). Similar results were obtained comparing IL-2Rα[−] and IL-2Rα^{+} YT cells (fig. S6, A and B). We further confirmed that the pH-selective behavior of Switch-2 is dependent upon IL-2Rα, observing its loss when the *Il2ra* gene was disrupted using CRISPR in preactivated cells (fig. S6C). Similar results were obtained in lactic acid−containing low-pH medium (fig. S6D). STAT5 signaling appeared to be more sensitive to acidic pH than other IL-2−driven signaling pathways, including extracellular signal−regulated kinase 1/2 (ERK1/2), Akt, and S6R, which displayed distinct levels of pH sensitivity (fig. S6, E to H). Stimulation of T$_{reg}$ cells with IL-2 and Switch-2 at pH 6.5 and 7.5 yielded comparable results to those obtained with preactivated CD8^{+} T cells (fig. S6I).

Switch-2 triggers more potent CD8^{+} T cell effector function at acidic pH

IL-2 drives T cell expansion and acquisition of effector functions, including the production of IFN-γ (*18*). Consistent with previous studies, we observed that acidic pH inhibits T cell expansion during the activation phase (fig. S7A) (*14*) and T cell effector functions (*19*). We therefore investigated the ability of CD8^{+} T cells stimulated with either IL-2 or Switch-2 to expand and produce effector cytokines in neutral and acidic pH conditions. CD8^{+} T cells were initially activated with anti-CD3 and anti-CD28 antibodies at pH 7.5 and then switched to medium at either pH 7.5 or 6.5 in the presence of IL-2 or Switch-2. Whereas IL-2 induced CD8^{+} T cell proliferation at pH 7.5, its effect was reduced at pH 6.5 (fig. S7, B and C). Switch-2, on the other hand, induced CD8^{+} T cell proliferation at both pH 7.5 and 6.5 (fig. S7, B and C). Considering that cytokine secretion is pH sensitive (*20–23*), we next studied cytokine secretion profiles by activated CD8^{+} T cells stimulated with IL-2 or Switch-2 at pH 7.5 or 6.5. Expansion in IL-2 elicited strong cytokine secretion by CD8^{+} T cells at pH 7.5 but almost fully lost its activity when cells were cultured at pH 6.5 (Fig. 3A). Switch-2, on the other

hand, elicited almost a mirror image in terms of pH selectivity, triggering stronger cytokine release by CD8^{+} T cells at pH 6.5 than at pH 7.5 (Fig. 3A). Moreover, at acidic pH, cytokines associated with effector function, such as IFN-γ, granulocyte-macrophage colony-stimulating factor (GM-CSF), and TNF, were up-regulated to a greater extent in cells expanded with Switch-2 than with IL-2 (Fig. 3A) (*24*). These results were confirmed using intracellular staining and flow cytometry (Fig. 3B and fig. S7, D and E).

To further define the effects of extracellular acidic pH on IL-2 activity at the molecular level, we performed RNA sequencing (RNA-seq) analysis on CD8^{+} T cells after 4 hours of stimulation with IL-2 variants in neutral or acidic pH conditions. Principal components analysis (PCA) of global gene expression profiles showed that cells treated with Switch-2 at pH 7.5 and 6.5 grouped together with cells treated with IL-2 at pH 6.5 and 7.5, respectively (Fig. 3C). In keeping with these results, gene set enrichment analysis (GSEA) showed that differentially expressed genes between Switch-2− and IL-2−stimulated cells at pH 6.5 were significantly enriched for IL-2 signature genes (*25*) generally induced by IL-2 at pH 7.5 (fig. S8A). These data further support the preferential activity of Switch-2 in acidic versus neutral pH. To identify IL-2−driven genes most sensitive to the effects of pH, we compared IL-2− and Switch-2−driven genes in CD8^{+} T cells cultured at pH 7.5 and 6.5. Whereas the number of IL-2−induced genes at neutral pH was severely attenuated at acidic pH, the number of genes induced by Switch-2 at neutral and acidic pH was comparable (fig. S8B). Differentially expressed genes were grouped into nine unique clusters (Fig. 3D and data file S1), with clusters 1 and 2 enriched in immune-related gene sets, including those involved in IL-2−STAT5 signaling (fig. S8C). Cluster 2 comprised IL-2−driven genes whose expression levels were significantly reduced at acidic pH (Fig. 3D). Switch-2, on the other hand, induced up-regulation of these genes at acidic pH while exhibiting weak activity at neutral pH (Fig. 3D). Cluster 2 included genes associated with T cell activation and effector function (*Hk2*, *Ifng*, *Il2ra*, *Il18r1*, *Ccl17*, *Cxcl10*, *Gzma*, and *Gzmb*) (Fig. 3E and fig. S8, D to F) (*18, 26, 27*). Some IL-2−induced genes, such as *Bcl2* and *Cish*, show less sensitivity to changes in pH, agreeing with our data showing that pH differentially affects IL-2 signaling (Figs. 2H and 3E and fig. S6, E to G). Together, these data support the notion that acidic pH limits IL-2−induced gene expression programs within CD8^{+} T cells and that the pH-selective activity of Switch-2 is reflected in the global gene expression changes it induces at acidic and neutral pH.

A pH-selective effect of Switch-2 versus IL-2 on STAT5 signaling within murine CD8^{+} T cells could be observed in vitro (fig. S9A). We next characterized binding and signaling activity of Switch-2 versus IL-2 in vivo. IL-2 binding is followed by rapid internalization of the IL-2−IL-2R complex (*28*). To trace IL-2 binding and/or uptake in vivo, we administered Alexa Fluor 647 (AF647)−labeled Fc-IL-2 and Switch-2 to B16.SIY tumor−bearing mice and analyzed its binding/uptake by CD8^{+} T cells 30 min after the injection of the labeled IL-2 on day 11, when there was no difference in tumor size between IL-2− and Switch-2−treated mice. We found that IL-2 was preferentially taken up by IL-2Rα^{+} CD8^{+} T cells in peripheral blood and lung compared with those found within the tumor or tumor-draining lymph nodes (tdLNs), which are considered acidic niches (Fig. 3F and fig. S9, B to F) (*29*). By contrast, Switch-2 was preferentially taken up by IL-2Rα^{+} CD8^{+} T cells within the tumor and tdLNs compared with those in peripheral blood and lung (Fig. 3F
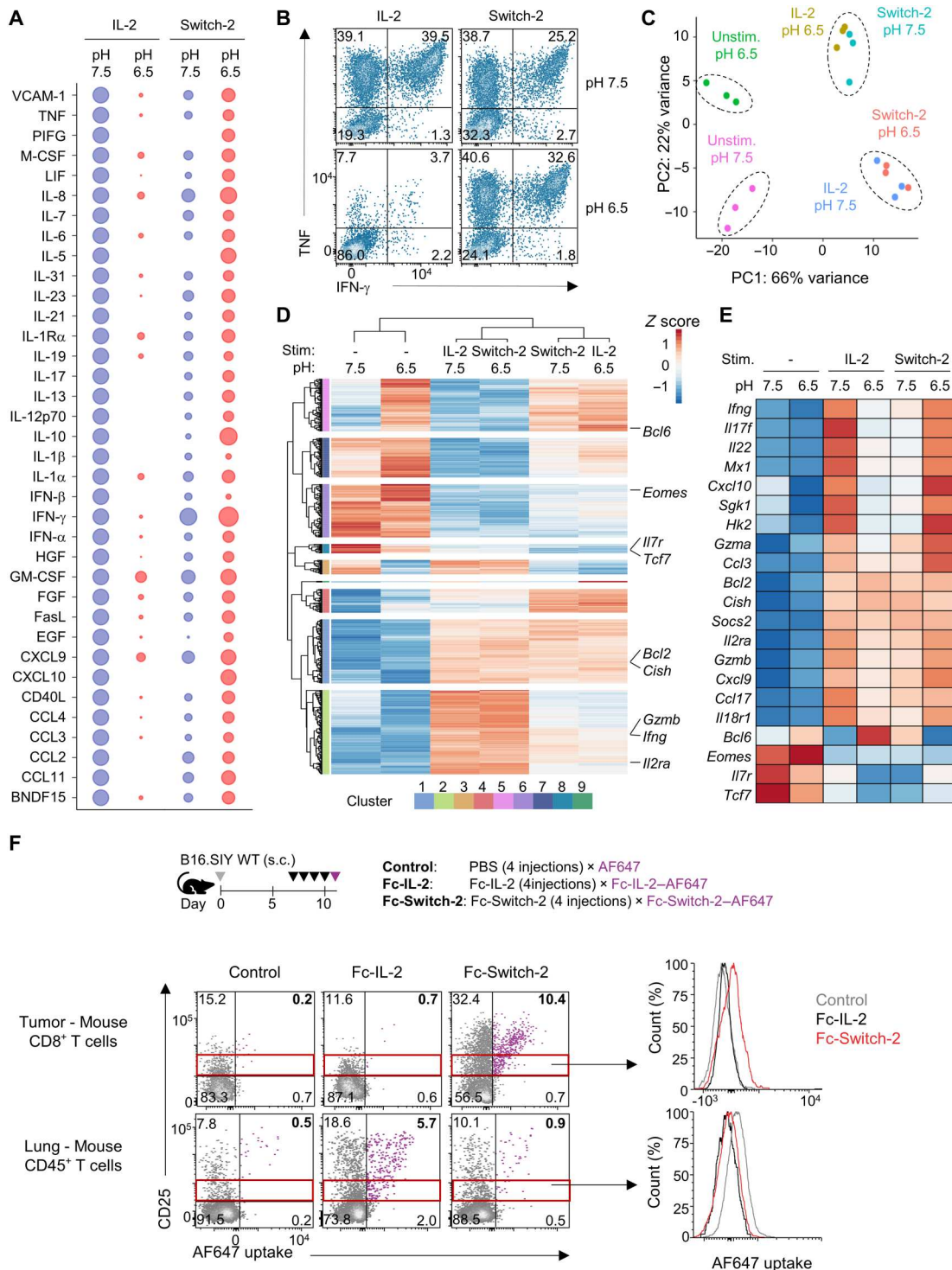
Fig. 3. The IL-2 mutein Switch-2 is preferentially active at acidic pH. (**A** and **B**) Analysis of cytokine expressed by preactivated CD8^{+} T cells after 3 days of culture at pH 7.5 or 6.5 in the presence of 10 nM IL-2 or Swtich-2. Cells were stimulated with phorbol 12-myristate 13-acetate (PMA)/ionomycin, and the supernatant of stimulated cells was analyzed by Luminex assay (A). The bubbles represent the amount of the released cytokines that has been normalized to control condition (IL-2, pH 7.5 = 100). (B) Dot plot showing the expression of IFN-γ and TNF in one of five representative donors. (**C**) PCA of RNA-seq data. Preactivated CD8^{+} T cells from three different donors were stimulated for 4 hours after resting overnight. PC, principal component. (**D** and **E**) Heatmap of the 476 top variable and significant genes (D) and of a set of T cell–specific genes (E). Gene expression is represented as z score. (**F**) IL-2Rα–dependent uptake of labeled Fc-IL-2 and Fc-Switch-2 in CD8^{+} T cells from mouse tumor and lung (left). In the right panel, the AF647 uptake within cells expressing similar levels of IL-2Rα (red gate in the left panel) is shown. s.c., subcutaneous.

and fig. S9, B to F). Moreover, by selecting for each condition CD8+ TILs expressing comparable levels of IL-2Rα, it is possible to observe that Switch-2 uptake by CD8+ TILs is stronger than IL-2 uptake, opposite to what we observed in the lung (Fig. 3F). IL-2Rα is a direct target of IL-2–induced pSTAT5. Correspondingly, in contrast to IL-2, Switch-2 treatment led to higher IL-2Rα expression on CD8+ T cells within tumor and tdLNs compared with blood and lung CD8+ T cells. Furthermore, in line with these data, Fc-IL-2 induced STAT5 phosphorylation preferentially in CD8+ T cells in the blood, whereas Fc-Switch-2 triggered STAT5 phosphorylation to a greater extent in the tumor and tdLN (fig. S9, G to L). Overall, these observations confirm the preferential in vivo activity of Switch-2 within acidic pH tissue environments.

Switch-2 elicits potent antitumor immune responses

High-dose IL-2 treatment can activate cytotoxic T and NK cell–mediated tumor killing, resulting in complete responses in about 7% of metastatic melanoma patients treated (30). However, its therapeutic efficacy is limited by poor activation of TILs within the TME. Our data demonstrated that intratumoral acidosis profoundly limits IL-2 activity within the TME (Fig. 1, C to K, and fig. S2). A large number of TILs within the tumor are dysfunctional (31). TILs isolated from tumors can be reactivated and expanded in vitro in the presence of IL-2. These data suggest that improper targeting and function of IL-2 within the TME might limit its in vivo efficacy. Given its enhanced activity at acidic pH, we tested the therapeutic efficacy of Switch-2 in four different tumor models. Switch-2 therapy led to stronger antitumor responses compared with IL-2 in the immunogenic MC38 colon carcinoma model, with more than one-third of animals achieving full remission (Fig. 4A and fig. S10, A and B). The cured animals rejected a subsequent rechallenge with MC38, demonstrating the induction of durable antitumor immunity by Switch-2 (Fig. 4B). In the 4T1 mammary cancer model, Fc-Switch-2 treatment significantly reduced the rate of tumor growth, whereas Fc-IL-2 had a minimal effect (Fig. 4C and fig. S10, C to F). Similar results were observed in the B16.SIY tumor model, where Fc-Switch-2 therapy significantly delayed tumor growth and increased survival (Fig. 4D and fig. S10, G and H). When Fc-Switch-2 therapy was combined with sodium bicarbonate treatment, the beneficial antitumor effect of Switch-2 was completely abrogated, further supporting the pH-switchable nature of Switch-2 in vivo (fig. S10, I to K). Moreover, the combination of anti–PD-L1 and Switch-2 treatment controlled established B16.SIY tumors more effectively than anti–PD-L1 and IL-2 treatment alone (fig. S11). Overall, these data demonstrate potent antitumor efficacy of Switch-2 in a variety of solid tumor models.

Previous studies have shown that lactic acidosis in tumors is less prevalent in small tumors such as early metastatic lesions (32). Thus, we investigated the effect of Switch-2 on antitumor immunity to lung metastases. Mice were intravenously injected with B16-F10-mCherry-OVA tumor cells and treated with IL-2 or Switch-2 therapy for 5 days. Both Fc-IL-2 and Fc-Switch-2 induced robust antitumor responses (fig. S12, A to C) with concomitant increases in the frequency of lung SIINFEKL peptide:major histocompatibility complex (MHC) tetramer–binding CD8+ T cell populations compared with the untreated group, although the relative frequency of CD8+ and Treg cells remained unchanged (fig. S12, D to G). Furthermore, the number of NK cells in tumor-bearing lungs was significantly increased by Fc-IL-2 and Switch-2 treatment, although

Switch-2 had a stronger effect (fig. S12H). Overall, these data reveal potent antitumor efficacy of both IL-2 and Switch-2 in driving immunity to early metastatic lesions.

To gain mechanistic insight into how Switch-2 leads to more potent antitumor responses, we characterized TILs and draining LN cells using the B16.SIY model using flow cytometry (Fig. 4, E to H, and fig. S13). Switch-2 and IL-2 triggered a small but not statistically significant increase in the CD8/Treg ratio as compared with phosphate-buffered saline (PBS)–treated controls (fig. S13, A to D). Switch-2, on the other hand, induced greater CD8+ T cell proliferation with a concomitant increase in the frequency of SIY antigen-specific CD8+ TIL and an increase in the frequency of infiltrating NK cells (Fig. 4, E and F, and fig. S13, E and F), a feature of effective IL-2 antitumor responses. This was accompanied by greater IFN-γ and TNF production by CD8+ T cells in Switch-2–treated animals (Fig. 4, G and H, and fig. S13, G and H). A higher fraction of CD8+ TILs in Switch-2–treated animals had a CD44+ effector phenotype, yet no major changes were observed in the levels of the exhaustion markers PD-1 and TIM3 compared with IL-2–treated animals (fig. S13, I to M). Similar results were obtained in tdLN, including increased frequencies of tumor-specific CD8+ T cells upon Switch-2 treatment versus IL-2 (fig. S14), consistent with our previous data demonstrating superior activity of Switch-2 in LNs (fig. S9, D and E). In agreement with these observations, FTY720 treatment, which inhibits immune cell egress from LNs, resulted in reduced antitumor responses by both IL-2 and Switch-2 (fig. S14, H to K). However, Switch-2 treatment retained higher activity than IL-2 treatment in combination with FTY720 administration, supporting the idea that Switch-2 is more active than IL-2 within the TME. Overall, these data indicate that the superior antitumor activities of Switch-2 are mediated via induction of effector CD8+ T cell responses.

To gain deeper insight into how Switch-2 regulates CD8+ TILs, we performed single-cell RNA-seq analysis of TILs from B16.SIY tumors treated with Fc-IL-2 or Fc-Switch-2. Clusters 5 and 6 contained cytotoxic CD8+ T cells with a higher frequency of Klrd1 (CD94) and Gzma expression, respectively, whereas both clusters expressed Itgb1, which encodes CD29 (Fig. 5, A and B; fig. S15, A and B; and data file S2) (33–35). We observed that the distribution of the CD8+ TILs from the IL-2– and Switch-2–treated mice was mostly overlapping and distinct from the PBS group (fig. S15C) and characterized by a higher proportion of proliferating cells (fig. S15D). However, Switch-2 treatment caused an increase in the frequency of cytotoxic CD8+ T cells forming clusters 5 and 6 (Fig. 5C). Analysis of differentially expressed genes between Switch-2 versus IL-2 groups confirmed that Switch-2 treatment increased expression of genes associated with cytotoxic T cell function (Fig. 5D and data file S3).

Reduced systemic toxicity upon Switch-2 therapy

A major limitation of current IL-2 therapies is their high systemic toxicity, characterized by vascular leak syndrome (36). We hypothesized that Switch-2 therapies would be less toxic due to its low activity at neutral pH found in peripheral tissues. To test this, we subjected mice to high-dose therapy with the two IL-2 variants. We found that high IL-2 doses induced pulmonary edema as indicated by increased wet weight of lungs following treatment, whereas high-dose Switch-2 therapy caused substantially less pulmonary edema and vascular permeability (Fig. 6, A to C). This was
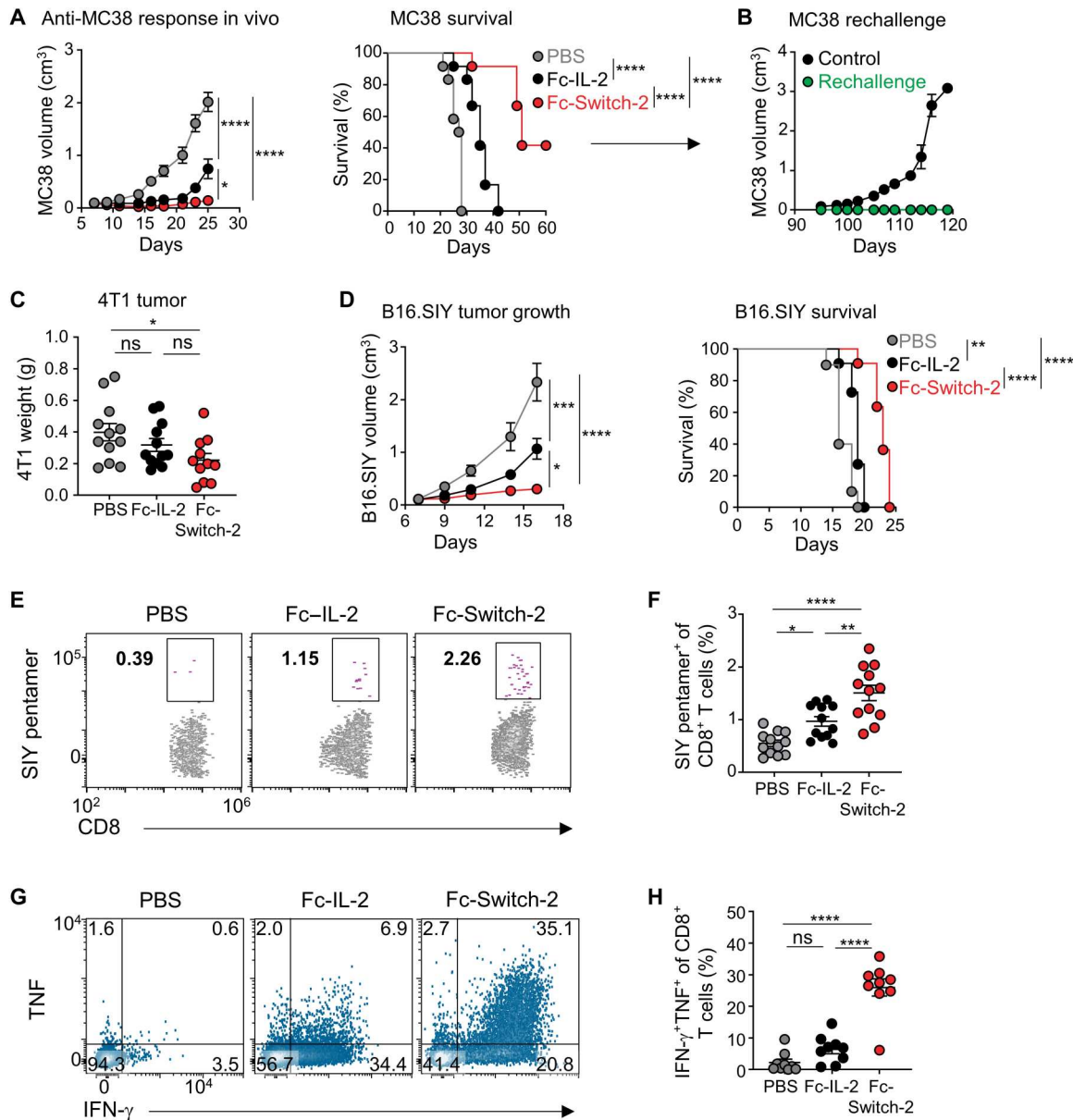
Fig. 4. Switch-2 therapy stimulates potent antitumor immunity and tumor control. (**A**) Tumor growth and survival curve of MC38-bearing mice (*n* = 12). (**B**) Tumor volume in MC38-rechallenged and age-matched control mice (*n* = 5). (**C**) Weight of 4T1 tumor. (**D**) Tumor growth and survival curve of B16.SIY WT–bearing mice (*n* = 10 for PBS, *n* = 12 for Fc-IL-2 and Fc-Switch-2). (**E** and **F**) Representative dot plot (E) and percentages (F) of antigen-specific CD8+ T cells in B16.SIY WT–bearing mice (*n* = 12). (**G** and **H**) Representative dot plot (G) and percentages (H) of TNF and IFN-γ expression in CD8+ T cell infiltrating B16.SIY WT tumor (*n* = 9). Each symbol represents a single mouse (C and F) or two mice pooled together (H), and data are the pooled results of two (A to F) or three independent experiments (H). Significance was determined by one-way ANOVA with Tukey's correction [A (left), C, D (left), F, and H] or by the log-rank test with Bonferroni's correction (A and D, right).

paralleled by reduced activity of Switch-2 in the periphery and lungs in mice injected with Switch-2 compared with IL-2 (fig. S9, D to I) (*29*) as well as lower percentages of NK cells in the periphery in mice injected with Switch-2 (Fig. 6, D and E). On the other hand, we found that Switch-2 increased the numbers of NK cells in the LNs to a higher extent than IL-2 (Fig. 6F). These data further demonstrate that Switch-2 displayed biased activity toward acidic pH tissue environments in vivo, thus leading to strong antitumor activities with minimal peripheral toxicity.

DISCUSSION

Collectively, these data demonstrate that cytokines are exquisitely sensitive to the pH of the tissue in which they operate. The practical implications of these findings are significant. By exploiting directed evolution, we improved the tissue-specific activity, efficacy, and systemic toxicity profile of IL-2, defining Switch-2 as a potential new immunotherapy for cancer, alone or in combination with checkpoint blockade or adoptive cell therapy.

Now, most new IL-2 therapeutics are focused on biasing the activity of IL-2 toward its dimeric receptor, which consists of IL-2Rβ
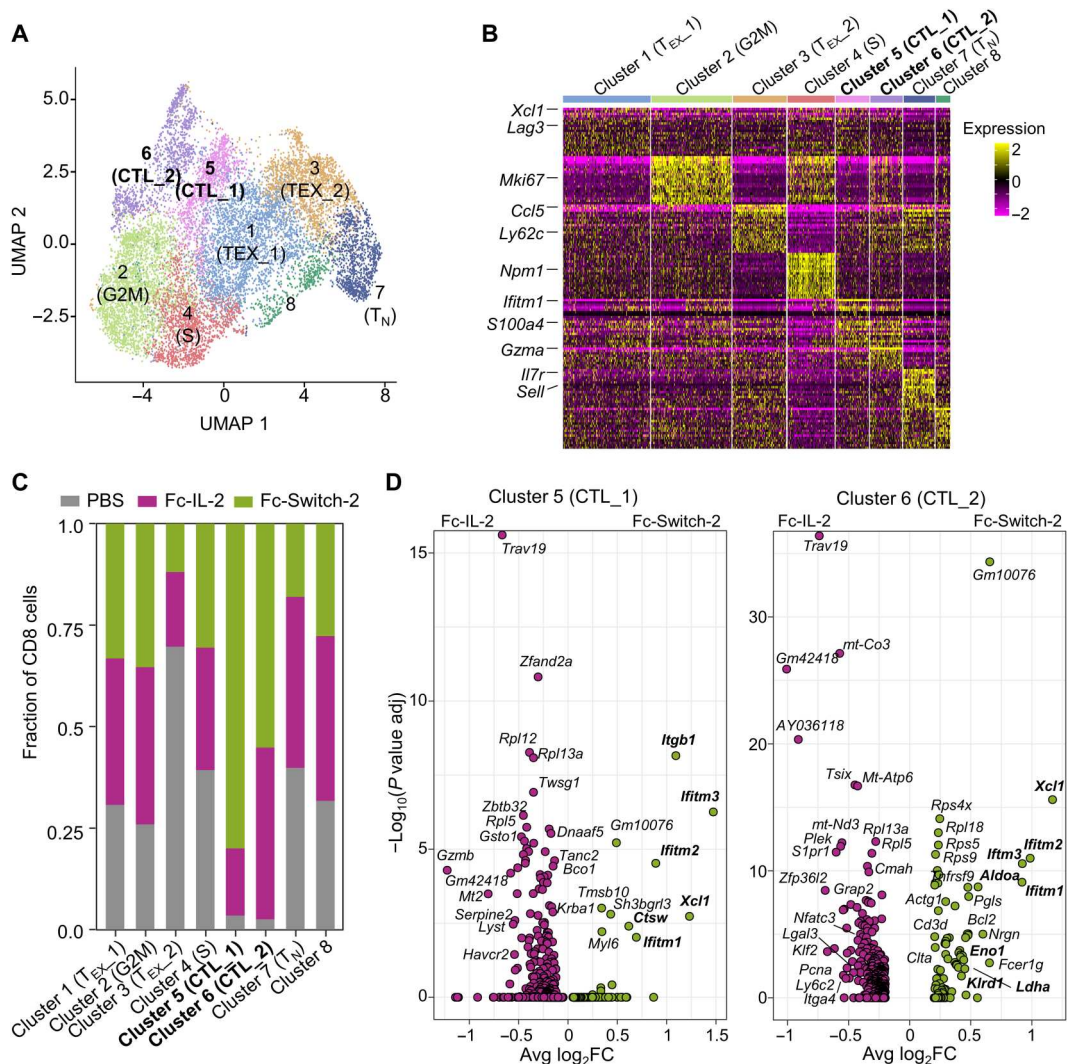
Fig. 5. scRNA-seq reveals induction of potent cytotoxic CD8+ cell responses within tumors after Switch-2 therapy. (**A**) UMAP from scRNA-seq colored by cluster. (**B**) Heatmap of CD8+ T cell clusters depicting the top 20 differentially expressed genes of each eight clusters. (**C**) Bar plot of the proportion of each sample in the different clusters normalized by the total number of cells of each sample. (**D**) Volcano plot of the differentially expressed genes in Fc-Switch-2 versus Fc-IL-2 sample in clusters 5 and 6. FC, fold change.

and IL-2Rγ, and away from its high-affinity trimeric receptor, which includes IL-2Rα. These new IL-2 therapies stimulate NK cells and certain subsets of T cells expressing the dimeric, and not the trimeric, form of the receptor. However, this approach fails to exploit expression by highly activated tumor-specific T cells of both IL-2Rα and IL-2Rβ. In addition, this approach expands peripheral NK cells, which have been shown in mice to cause vascular leak syndrome (*37*). Switch-2 represents a highly differentiated therapy in which the balance of signaling has been adjusted to favor the trimeric form of the IL-2 receptor only in the acidic tumor environment while significantly reducing its activity in peripheral blood. Switch-2 challenges the dogma that selective binding to the dimeric IL-2 receptor is the optimal approach for tumor therapy and improves IL-2 bioactivity within the TME while avoiding IL-2–mediated toxicity. Although here we focus on IL-2, our data show that pH sensitivity might be a generalizable phenomenon relevant to a broad spectrum of cytokines; however, more in-depth studies are

necessary to confirm this observation. Our findings therefore provide a basis for exploring the effect of pH and other physicochemical characteristics of the extracellular environment on cytokine activity and function in healthy and diseased tissues.

MATERIALS AND METHODS
Cell culture and medium
B16.SIY WT and B16.SIY LDHA/B DKO (provided by M. Kreutz, University of Regensburg) (*13*), IL-2Rα⁻ YT (provided by J. Spangler, John Hopkins University) and IL-2Rα⁺ YT (*38*), and 4T1 [American Type Culture Collection (ATCC), CRL-2539] cells were cultured in RPMI 1640 with GlutaMAX supplemented with 10% fetal bovine serum (FBS) and penicillin/streptomycin. IL-2Rα⁻ and IL-2Rα⁺ YT cells were validated by Eurofins. MC38 cells (Kerafast, ENH204-FP) were cultured in Dulbecco's modified Eagle's medium (DMEM) with GlutaMAX supplemented with 10%
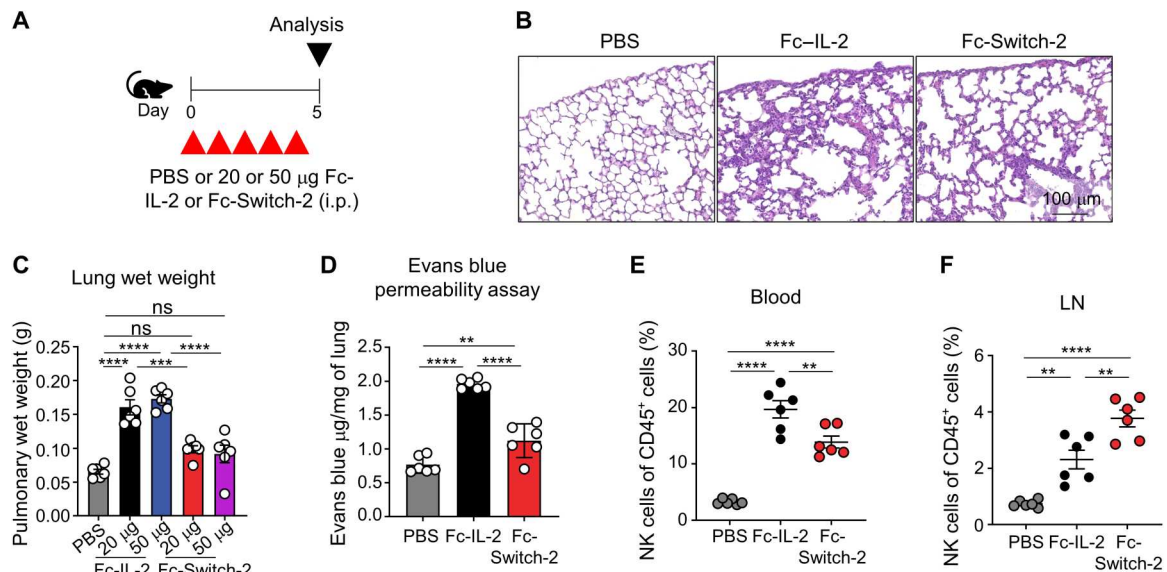
Fig. 6. Switch-2 drives reduced toxicity in systemic tissues. (**A**) Mice were treated for 5 days with intraperitoneal (i.p.) injections of 100 μl of PBS or 20 or 50 μg of Fc-IL-2 or Fc-Switch-2 for 5 days. (**B**) Representative images of lung tissue stained with hematoxylin and eosin after treatment with Fc-IL-2 and Fc-Switch-2. (**C** and **D**) Pulmonary edema evaluated by lung wet weight (C) and amount of Evans blue per milligram of lung tissue (D) after treatment with Fc-IL-2 and Fc-Switch-2 (n = 6). (**E** and **F**) Percentage of NK cells in blood (E) and LN (F) of mice treated with either PBS, 20 μg of Fc-IL-2, or 20 μg of Fc-Switch-2. (B to F) Each symbol represents a single mouse, and data are the pooled results of two independent experiments. Significance was determined by one-way ANOVA with Tukey's correction.

FBS, penicillin/streptomycin, 0.1 mM minimum nonessential amino acids, 1 mM sodium pyruvate, and 10 mM Hepes. B16-F10-mCherry-OVA tumor cells (provided by M. Krummel, University of California San Francisco) were passaged in DMEM supplemented with 10% FBS and penicillin/streptomycin. HeLa cells (ATCC, CCL-2) stably transfected with SNAPf–IL-2Rα were cultured in MEM supplemented with Earle's balanced salts, glutamine, 10% FBS, nonessential amino acids, and Hepes buffer without addition of antibiotics. For baculovirus preparation and protein production, *Spodoptera frugiperda* (Sf9; Thermo Fisher Scientific, 12659017) and *Trichoplusia ni* (High Five; Thermo Fisher Scientific, B85502) cells were cultured in Sf-900 III SFM medium (Invitrogen, 12658027) and in Insect Xpress medium (Lonza, BELN12-730Q), respectively. Human T cells were cultured in RPMI 1640 with GlutaMAX (Gibco, 61870036) supplemented with 10% FBS, minimum nonessential amino acids, 1 mM sodium pyruvate, and penicillin/streptomycin. When the pH of the medium was adjusted to conduct short- or long-term experiments, HCl was used to acidify the medium, and 20 mM Hepes (pH 6.5) was added to maintain a stable pH of 6.5 in the presence of 5% CO_2. An equivalent amount of Hepes (pH 7.5) was added to the medium at pH 7.5. In the case of murine T cells, the medium was further supplemented with 50 mM β-mercaptoethanol.

Protein production
Human IL-2 (residues 1 to 133) and Switch-2 were cloned into the pFB-CT10HF vector in frame with the N-terminal gp67 and the C-terminal histidine tag; human IL-2Rα ectodomain (residues 1 to 217) was cloned in the same vector with a C-terminal biotin acceptor peptide (BAP)–LNDIFEAQKIEWHW followed by a histidine tag; for in vivo experiments, the Fc portion of human IgG4 was cloned at the N terminus of IL-2 and Switch-2. Proteins were produced using the baculovirus expression system. Briefly, vectors were

recombined in DH10Bac bacteria (Gibco), and the generated bacmid was used to generate the baculovirus. Baculovirus was produced and amplified in Sf9 cells and used to infect High Five cells for protein expression. Two days after infection, His-Pur Ni–nitrilotriacetic acid (NTA) resin (Invitrogen, 88222) was used to capture the proteins released in the cell culture supernatant. Proteins were purified by size exclusion chromatography on a Superdex 75 Increase column (GE Healthcare, 29-1487-21). Proteins were conserved in 10 mM Hepes (pH 7.2) and 150 mM NaCl (Hepes-buffered saline). In the case of IL-2Rα, the protein was reduced with 10 mM cysteine, alkylated with 20 mM iodoacetamide (*39*), and biotinylated with BirA ligase in the presence of 100 μM biotin. For analysis of in vivo IL-2 uptake, Fc-IL-2 and Fc-Switch-2 were labeled with fourfold excess of Alexa Fluor 647 NHS Ester (Thermo Fisher Scientific, A20006). Proteins used for in vivo experiments were confirmed endotoxin-free by the Pierce LAL Chromogenic Endotoxin Quantification Kit (Thermo Fisher Scientific, 88282).

For microscopy experiments, IL-2 and Switch-2 were cloned into the pMAL vector in frame with N-terminal maltose-binding protein (MBP), a ybbR tag (DSLEFIASKLA peptide) (*40*), and a C-terminal histidine tag. BL21 *Escherichia coli* cells were used to express the protein upon overnight induction with 1 mM isopropyl-β-D-thiogalactopyranoside (IPTG) at 20°C. The periplasmic fraction was isolated by osmotic shock, and recombinant proteins were captured by His-Pur Ni-NTA resin. Proteins were purified by size exclusion chromatography on a Superdex 75 Increase column. Site-specific enzymatic labeling via the ybbR tag was performed using coenzyme A conjugated with DY647P1 maleimide (DY647, Dyomics) and the phosphopantetheinyl transferase Sfp as described previously (*41*).

Human T cell isolation and culture

Peripheral blood mononuclear cells (PBMCs) of healthy donors were isolated from buffy coats (Etablissement Français du Sang) by density gradient centrifugation using Pancoll human (PAN-Biotech, P04-60500). PBMCs (200×10^6) were stained with 15 μl of anti-human CD8 fluorescein isothiocyanate (FITC) antibody (clone HIT8a; BioLegend, 300906) for 15 min at 4°C, washed, and incubated with 70 μl of anti-FITC microbeads (Miltenyi, 130-048-701). CD8$^+$ T cells were isolated by magnetic separation using LS columns (Miltenyi, 130-042-401) and activated for 3 days in complete medium using coated anti-human CD3 antibody (clone OKT3; BioLegend, 317326) and soluble anti-human CD28 antibody (2 μg/ml; clone CD28.2; BioLegend, 302934). Activation was always carried out at neutral pH 7.5 except when specifically indicated. For proliferation assay, CD8$^+$ T cells were labeled with CellTrace Violet (Thermo Fisher Scientific, C34557) before T cell activation following the manufacturer's protocol. For mRNA purification, activated CD8$^+$ T cells were rested overnight, transferred in complete medium at pH 7.5 or 6.5, and stimulated for 4 hours with 10 nM IL-2 or Switch-2. Activated CD8$^+$ T cells used for analyzing cytokine expression and for secretome analysis were cultured for 3 days in medium at pH 7.5 or 6.5 in the presence of 10 nM IL-2 or Switch-2 and subsequently stimulated for 4 hours. Cell stimulation cocktail containing transport inhibitors (eBioscience, 00-4975-93) was used for cytokine expression analysis by flow cytometry. Supernatant for Luminex analysis was collected upon stimulation with cell stimulation cocktail (eBioscience, 00-4970-93). CD4$^+$ cells were isolated using 40 μl of anti-human CD4 FITC antibody (clone A161A1; BioLegend, 357406) following the same protocol as CD8$^+$ T cell isolation.

Signaling experiments

IL-2 signaling was evaluated on YT cells, freshly isolated CD8$^+$, preactivated CD8$^+$ T cells after resting overnight, and on T$_{reg}$ cells from freshly isolated CD4$^+$ T cells. Cells were stimulated for 15 min with the indicated amount of IL-2 or Switch-2 in medium at pH 7.5 or 6.5. In the case of time-course experiments, cells were stimulated for 6 hours, 3 hours, 2 hours, 1 hour, 30 min, and 15 min with 10 nM or 10 pM IL-2. IL-2 signaling in T$_{reg}$ cells was evaluated after 15-min stimulation of freshly isolated total CD4 cells.

Sample processing and staining for flow cytometry analysis

Cells were incubated with a Zombie aqua fixable viability kit (BioLegend, 423101) for 20 min at 4°C and then stained for surface markers for 30 min at 4°C in magnetic-activated cell sorting (MACS) buffer (Miltenyi, 130-091-221) using anti-human CD8 FITC, anti-human CD3 BV711 (clone UCHT1; BioLegend, 300463), or anti-human CD25 allophycocyanin (APC) (clone M-A251; BioLegend, 356110). For the analysis of cytokine expression, cells stained for surface markers were subsequently fixed and permeabilized using a BD Cytofix/Cytoperm kit (BD Biosciences, 554714). Anti-human IL-2 BV421 (clone MQ1-17H12; BioLegend, 500328), anti-human TNF-α phycoerythrin (PE)/Dazzle 594 (clone Mab11; BioLegend, 502946), and anti-human IFN-γ APC (clone B27; BioLegend, 506510) were used. All the antibodies were used at 1:100.

For dose-response and kinetic experiments, stimulated cells were immediately fixed with 2% paraformaldehyde for 15 min at room temperature (RT). Cells were subsequently washed with PBS and permeabilized with ice-cold methanol for 30 min on ice and fluorescently barcoded as previously described (*42*). In brief, individual wells were stained with a combination of different concentrations of Pacific Blue (Thermo Fisher Scientific, 10163) and DyLight 800 NHS dyes (Thermo Fisher Scientific, 46421). Sixteen barcoded samples were pooled together and stained for surface markers with anti-human CD3 BV711, anti-human CD4 FITC, or anti-human CD8 FITC and for phosphoproteins with anti-STAT5 PE (1:100; clone 47/Stat5; BD Biosciences, 612567), anti-ERK1/2 AF647 (1:100; clone 4B11B69; BioLegend, 677504), anti-Akt AF647 (1:50; clone 193H2; Cell Signaling Technology, 2337S), and anti-S6R PE (1:100; clone D57.2.2E; Cell Signaling Technology, 5316S) in MACS buffer for 1 hour at RT. In the case of signaling experiments on T$_{reg}$ cells, samples were washed and stained with 1:10 anti-human FoxP3 AF647 (clone 259D/C7; BD Biosciences, 560045) using the FoxP3/transcription factor staining buffer set (eBioscience, 00-5523-00).

For in vivo analysis of STAT5 phosphorylation, tdLN and tumor samples were mechanically disrupted on a cell strainer directly in the Lyse/Fix buffer (BD Biosciences, 558049). Blood was immediately diluted in the Lyse/Fix buffer. Samples were fixed for 7 min, washed, and permeabilized with Perm buffer III (BD Biosciences, 558050) for 30 min. Cells were subsequently stained for 1 hour at RT with anti-mouse CD3 peridinin chlorophyll protein (PerCP)–Cy5.5 (1:100; clone 17A2; BioLegend, 100218), anti-mouse CD8 PE-Cy7 (clone 53-6.7; BioLegend, 10722), anti-mouse CD45 BV711 (1:200; clone 30-F11; BioLegend, 103147), and anti-STAT5 PE (1:30). For the other analysis, single-cell suspension of murine lungs and LNs was obtained by mechanical disruption on a cell strainer. Red blood cells were lysed using RBC lysis buffer for mouse (Alfa Aesar, J62150). For phenotypical analysis, B16.SIY subcutaneous tumor and lungs from B16-F10-mCherry-OVA metastatic model were cut in small pieces and digested with collagenase (1 mg/ml; Sigma-Aldrich, C6885) and deoxyribonuclease I (0.1 mg/ml; STEMCELL Technologies, 07470) in RPMI/25 mM Hepes for 50 min at 37°C under shaking. The cell suspension was passed through a cell strainer and subsequently resuspended in PBS at 10^6 cells/ml. An equal volume of Lympholyte-M (Cedarlane, CL5031) was underlaid, and the samples were centrifuged at 1200*g* for 20 min. The lymphocyte layer was collected, washed with PBS, resuspended in 4 ml of 37% isotonic solution of Percoll (Cytiva, 17089101), and centrifuged at 600*g* for 10 min. In the case of the lungs from the metastatic melanoma model, the samples were subsequently incubated for 3 min with the RBC lysis buffer. For the in vivo IL-2 tracking experiments, samples were mechanically disrupted on a cell strainer. For analysis of cytokine expression, the samples from two mice were pooled together and cells were stimulated for 4 hours at 37°C with Cell Stimulation Cocktail (Thermo Fisher Scientific, 00-4675-93). After treatment with TruStain FcX (anti-mouse CD16/32) antibody (BioLegend, 101320), samples were incubated for 10 min at RT with R-PE–labeled Pro5 MHC Pentamer (ProImmune) specific for H-2Kb SIYRYYGL or with BV421-H-2 K(b)/SIINFEKL (OVA$_{257-268}$) MHC Tetramer (provided by NIH Tetramer Core Facility), washed, and then stained for surface and intracellular markers following the same procedure described before. The following antibodies were used: anti-mouse CD3 PerCP-Cy5.5 (1:200; clone 17A2; BioLegend, 100218), anti-mouse CD4 BV605 (1:200; clone RM4-5; BioLegend, 100548), anti-mouse CD4 AF700 (1:200; clone GK1.5; BioLegend,

100430), anti-mouse CD8 AF488 (1:200; clone 53-6.7; BioLegend, 100723), anti-mouse CD45 BV711 (1:200; clone 30-F11; BioLegend, 103147), anti-mouse CD122 PE/Dazzle 594 (1:200; clone TM-b1; BioLegend, 123217), anti-mouse PD-1 BV785 (1:100; clone 29F-1A12; BioLegend, 135225), anti-mouse TIM3 BV421 (1:50; clone RMT3-23; BioLegend, 119723), anti-mouse NK1.1 BV605 (clone PK136; BioLegend, 108739), anti-mouse FoxP3 PE (clone FJK-16s; eBioscience, 12-5773-82), anti-mouse Ki67 PE-Cy5 (1:100; clone SolA15; eBioscience, 15-5698-82), anti-mouse NK1.1 BV605 (1:200; clone PK136; BioLegend, 108739), anti-mouse CD44 APC-Cy7 (1:50; clone IM7; BioLegend, 103027), CD62L APC (1:20; clone MEL-14; BioLegend, 104412), anti-mouse CD25 BUV395 (1:100; clone PC61; BD Biosciences, 564022), anti-mouse TNF-α BV605 (1:200; clone MP6-XT22; BioLegend, 506329), and anti-mouse IFN-γ APC (1:200; clone XMG1.2; BioLegend, 505809). Flow cytometry was performed using an LSR Fortessa X20 (BD Biosciences) instrument, and data were analyzed with FlowJo software (TreeStar Inc., version 10) or with FCS Express 7 (De Novo Software).

Animal models
Six-week-old female C57Bl/6JRj mice (Janvier) were subcutaneously injected in the right flank with 3×10^4 B16.SIY WT or B16.SIY LDHA/B DKO or with 3.5×10^5 MC38 cells in PBS and Matrigel (1:1) (Corning, 356232). For the metastatic melanoma model, 6×10^5 cells in 150 µl of PBS were intravenously injected. Fc-IL-2 or Switch-2 (20 µg) was intraperitoneally administered from day 7, when the size of the subcutaneous tumor reached 100 mm³, until day 11. When indicated, mice were treated with 200 mM NaHCO₃ in the drinking water starting 3 days before tumor injection and until the end of the experiment (23). InVivoMAb anti-mouse PD-L1 (100 µg; clone 10F.2H11; Bio X Cell, BE0361) or In-VivoMAb rat IgG2b isotype control (Bio X Cell, BE0090) was intraperitoneally administered at days 7, 10, and 13. Treatment with 50 µg of FTY720 (Sigma-Aldrich, SML0700) was performed every 4 days by intraperitoneal injections starting from day 5 until the end of the experiment. In the case of the MC38 model, surviving mice were rechallenged at day 88 with subcutaneous injection of 3.5×10^5 in the left flank in parallel with control age-matched mice. 4T1 cells (10^5) were injected in 6-week-old female Balb/cByJRJ mice (Janvier) and treated with intraperitoneal injections of 20 µg of Fc-IL-2 or Fc-Switch-2 from days 7 to 13. Tumors were measured using a caliper, and tumor volume was calculated using the formula length × width²/2. For in vivo analysis of STAT5 phosphorylation and IL-2 uptake, mice were euthanized 30 min after the last injection of IL-2. In the case of IL-2 uptake studies, the last injection was performed using AF647-labeled Fc-IL-2 or Fc-Switch-2 or an equimolar amount of AF647 in the PBS-treated group. For the analysis of TILs, mice were euthanized at day 15 after tumor injection for the B16.SIY subcutaneous model or at day 16 for the B16-F10-mCherry-OVA metastatic model. For the toxicity test, 20 or 50 µg of Fc-IL-2 or Switch-2 was given for five consecutive days by intraperitoneal injections and mice were euthanized the day after the last injection. The blood vessel permeability in the lung was assessed by retro-orbital injection of 50 µl of Evans blue (50 mg/ml) 30 min before euthanizing the mice. Lungs were perfused with PBS, dried overnight at 80°C, weighted, and incubated overnight in 1.5 ml of formamide at 55°C. The amount of extracted dye was evaluated by measuring the optical density at 260 nm,

and nanograms of Evans blue per milligram of dry lung tissue was calculated. Pulmonary edema (pulmonary wet weight) was evaluated by measuring the wet weight after lung collection and subtracting the dry weight after the lungs were exsiccated overnight at 80°C. Animal experiments were conducted in accordance with the "Ministère de l'enseignement supérieur, de la recherche et de l'innovation" (protocol no. 19862-2019022809122912).

Generation and selection of IL-2 library
Adapting a previously described protocol for yeast display (43), we cloned IL-2 cDNA in the pCT302 vector for the expression in yeast. The IL-2 library was generated assembling eight overlapping primers, among which two of them contained the homology regions necessary for the combination with the pCT302 vector (table S1). Three of the primers had NDT codons (encoding for Gly, Val, Leu, Ile, Cys, Ser, Arg, His, Asp, Asn, Phe, and Tyr amino acids) used to randomly mutate Thr³⁷, Arg³⁸, Thr⁴¹, Phe⁴², Lys⁴³, Glu⁶⁰, Glu⁶¹, Glu⁶³, Leu⁶⁶, Glu⁶⁸, Val⁶⁹, Asp¹⁰⁹, and Glu¹¹⁰ residues. The polymerase chain reaction (PCR) product was further amplified using Lib Fw and Lib Rv primers (table S1), at a final concentration of 10 µM, to obtain at least 25 µg of DNA.

Saccharomyces cerevisiae strain EBY100 was transformed by electroporation with 25 µg of insert DNA and 5 µg of the linearized and purified plasmid. Transfected yeasts were grown in synthetic defined medium with casamino acids (SDCAA) medium for 1 day at 30°C and in synthetic defined medium with casamino acids and galactose (SGCAA) for 2 days at 20°C at each round of selection. The library, with a size of 5×10^7, was screened by MACS using an LS column (Miltenyi, 130-042-401): The first round of selection was carried out with 10^{10} cells, and the subsequent ones were carried out with 10^8 cells to ensure at least 10-fold coverage for each round. Biotinylated IL-2Rα ectodomain was used at different concentrations to select pH-resistant IL-2 variants: The first two rounds were performed using IL-2Rα tetramer at 100 nM in pH 5, and the third and fourth rounds were performed with 1 µM and 100 nM IL-2Rα monomer, respectively. IL-2Rα tetramers were generated by incubating IL-2Rα and streptavidin (SA)–AF647 at a ratio of 4:1.

Crystallography
Proteins were expressed and purified as described above. The CD25:Switch2 complex was formed by mixing CD25 at 32 µM with Switch-2 protein at a 20% excess based on molarity followed by dialysis overnight against 20 mM bis-tris (pH 6.0) and 150 mM NaCl. The complex was purified using a preequilibrated Superdex 75 (10/300 GL, Cytiva) gel filtration column. The final purified complex was concentrated to 7 mg/ml using a 30-kDa cutoff Amicon Ultracel device (Millipore). The sample was prepared for crystallization by filtration through a 0.2-mm centrifugal filtration device (Neobiotech). Crystallization was performed by hanging drop vapor diffusion in 24-well Linbro plates (Hampton Research) by mixing drops containing 0.75 µl each of reservoir and protein solution that was then equilibrated against 500 ml of reservoir solution. The reservoir solution consisted of 19% PEG 3350 (polyethylene glycol, molecular weight 3350), 0.2 M sodium tartrate dibasic dihydrate, and 10% glycerol, yielding a final pH of 6.9 in the crystallization drop. The plates were incubated at 18°C, and crystals were formed over the course of a week. The crystals were harvested with additional cryoprotection provided by passage through a

smear of Paratone-N (Hampton Research) on a glass slide and subsequent plunge cooling in LN_2.

Data were collected at Beamline I03 Diamond Light Source (UK) using an Eiger2 XE 16M detector (Dectris). The data were processed using Xia2/Dials (44) and scaled using aimless (45) from the CCP4 suite (46). Molecular replacement was performed using Phaser (47) with the IL-2 and CD25 coordinates from Protein Data Bank (PDB) entry 2B5I (39) used as the search model. One strong solution was found in space group $P322_1$, with a single complex present in the asymmetric unit. Refinement was performed using Phenix Refine (48) between cycles of manual analysis, and rebuilding was performed using Coot (49). MolProbity (50) was used for structure evaluation and validation. Full processing and refinement statistics are presented in table S2.

RNA-seq analysis

RNA of human CD8+ T cells was purified using a Quick-RNA Microprep kit (Zymo Research, R1051). Clean sequence reads were obtained by removing bad quality reads from raw data using fastp. Reads were removed when containing adapter, when containing more than 10% of uncertain nucleotides (N) in either R1 or R2, or when containing more than 50% low-quality nucleotides (base quality less than 5). Read mapping and quantification were performed by Novogene using STAR v2.6.1d with mismatch = 2 and FeatureCounts v1.5.0-p3 software with the GRCh38 human genome. Differential expression analysis was performed using DESeq2 (51), and heatmaps were realized with pheatmap R packages. GSEA analysis was performed using GSEA 4.1.0 and compared with the IL-2 gene signature described by Mitra et al. (25). Within the top 500 variable genes, 476 significantly differentially expressed genes [$P_{adj} < 0.05$, $\log_2$(fold change) > 0.6] were clustered by hierarchical clustering. Functional enrichment analysis was performed on clusters using the enricher function from clusterProfiler R packages (52) and hallmark gene sets v7.4 from MsigDB.

scRNA-seq sample preparation

Mice were euthanized the day after the end of the therapy, tumors were excised, and TILs were enriched using lymphocyte M density gradient protocol. Then, a MagniSort mouse CD8 T cell enrichment kit (Thermo Fisher Scientific, 8804-6822-74) was used to enrich for CD8+ TILs from the cell suspension. An equal amount of cell from each biological replicate (n = 3) was pooled together and stained using a Zombie aqua fixable viability kit, anti-mouse CD3 PerCP-Cy5.5, and anti-mouse CD8 PE (BioLegend, 100708). Live CD3+CD8+ cells were sorted and used for single-cell RNA-seq (scRNA-seq). A total of 13,000 cells were loaded on 10x Genomics Chromium system, and libraries were prepared with Chromium Next GEM Single Cell 3′ Reagent Kit v3.1 (dual index) following the manufacturer′s instructions.

scRNA-seq analysis

Raw sequencing data were processed and aligned to mouse genome (GRCm38) with 10x Genomic Cell Ranger pipeline (version 6.1.2) (53). Single-cell data were then analyzed using Seurat R package (version 4.1.0) (54). Low-quality cells with number of detected genes < 300 and mitochondrial gene RNA content > 7% and putative cell multiplets with number of detected genes > 6000 were excluded from the analysis. Single-cell count data were normalized, and genes with highly variable expression were identified using

SCTransform methods. Using CellCycleScoring function, each cell was associated with either G_1, S, or G_2-M cell cycle phase. Cell cycle association was done depending on expression score of genes related to each cell cycle phase in each cell. All used cell cycle genes were mouse versions of human genes provided in Seurat package. The 3000 most variable genes were used to compute 30 principal components with PCA. Shared nearest neighbor graphs were built using all principal components. Cells were then clustered according to shared nearest neighbor graphs using Louvain algorithm with resolution parameter set to 0.5. Embedding of cells in a two-dimensional (2D) space was computed with Unique Manifold Approximation and Projection (UMAP) on all principal components. Small clusters of cells with high expression of genes specific to myeloid, melanoma, or NK cells were removed from the dataset. Myeloid cell clusters were identified by high expression of *Cd74*, *Cd68*, and *Tyrobp*. A melanoma cancer cell cluster was identified by high expression of *Mlana*. An NK cell cluster was identified by high expression of *Ncr1*, *Klrb1c*, and *Tyrobp*. The remaining cells were reanalyzed using the exact same pipeline from normalization to 2D space embedding and setting resolution parameter to 0.4 for clustering. In total, 12,044 cells passed all filtering steps: 4045 from PBS sample, 1701 from Fc-IL-2 sample, and 6298 from Fc-Switch-2 sample.

Differentially expressed genes between groups of cells were determined using the Wilcoxon test. Only genes expressed in at least 10% of cells in either group and with at least an average absolute $\log_2$ fold change of 0.2 were tested. Multiple testing corrections for P values were done using Bonferroni correction based on the total number of genes in the dataset. Genes with adjusted $P < 0.05$ were considered differentially expressed.

Statistical analysis

Data are presented as means ± SEM of at least three independent experiments, and multiple-group comparisons were performed using one-way analysis of variance (ANOVA) with Tukey′s correction unless otherwise stated. Survival curves are represented as Kaplan-Meier curves, and statistical significance was determined by the log-rank test with Bonferroni′s correction. ns, not significant; $*P < 0.05$, $**P < 0.01$, $***P < 0.001$, and $****P < 0.0001$. All the analyses were performed using Prism 9 software (GraphPad).

Supplementary Materials

This PDF file includes:
Supplementary Methods
Figs. S1 to S15
Tables S1 and S2
References (55–66)

Other Supplementary Material for this manuscript includes the following:
Movies S1 to S5
Data files S1 to S3
MDAR Reproducibility Checklist

View/request a protocol for this paper from *Bio-protocol*.

REFERENCES AND NOTES

1. C. Gorby, J. Martinez-Fabregas, S. Wilmes, I. Moraga, Mapping determinants of cytokine signaling via protein engineering. *Front. Immunol.* **9**, 2143 (2018).

2. A. V. Villarino, Y. Kanno, J. R. Ferdinand, J. J. O'Shea, Mechanisms of Jak/STAT signaling in immunity and disease. *J. Immunol.* **194**, 21–27 (2015).

3. J.-X. Lin, W. J. Leonard, Fine-tuning cytokine signals. *Annu. Rev. Immunol.* **37**, 295–324 (2019).

4. I. Moraga, J. Spangler, J. L. Mendoza, K. C. Garcia, Multifarious determinants of cytokine receptor signaling specificity. *Adv. Immunol.* **121**, 1–39 (2014).

5. C. Schindler, D. E. Levy, T. Decker, JAK-STAT signaling: From interferons to cytokines. *J. Biol. Chem.* **282**, 20059–20063 (2007).

6. S. Mitra, W. J. Leonard, Biology of IL-2 and its therapeutic modulation: Mechanisms and strategies. *J. Leukoc. Biol.* **103**, 643–655 (2018).

7. S. A. Rosenberg, IL-2: The first effective immunotherapy for human cancer. *J. Immunol.* **192**, 5451–5458 (2014).

8. S. H. Ross, D. A. Cantrell, Signaling and function of interleukin-2 in T lymphocytes. *Annu. Rev. Immunol.* **36**, 411–433 (2018).

9. X. Wang, P. Lupardus, S. L. LaPorte, K. C. Garcia, Structural biology of shared cytokine receptors. *Annu. Rev. Immunol.* **27**, 29–60 (2009).

10. D. S. Vinay, E. P. Ryan, G. Pawelec, W. H. Talib, J. Stagg, E. Elkord, T. Lichtor, W. K. Decker, R. L. Whelan, H. M. C. S. Kumara, E. Signori, K. Honoki, A. G. Georgakilas, A. Amin, W. G. Helferich, C. S. Boosani, G. Guha, M. R. Ciriolo, S. Chen, S. I. Mohammed, A. S. Azmi, W. N. Keith, A. Bilsland, D. Bhakta, D. Halicka, H. Fujii, K. Aquilano, S. S. Ashraf, S. Nowsheen, X. Yang, B. K. Choi, B. S. Kwon, Immune evasion in cancer: Mechanistic basis and therapeutic strategies. *Semin. Cancer Biol.* **35**, S185–S198 (2015).

11. D. Hanahan, R. A. Weinberg, Hallmarks of cancer: The next generation. *Cell* **144**, 646–674 (2011).

12. C. Corbet, O. Feron, Tumour acidosis: From the passenger to the driver's seat. *Nat. Rev. Cancer* **17**, 577–593 (2017).

13. K. Renner, C. Bruss, A. Schnell, G. Koehl, H. M. Becker, M. Fante, A.-N. Menevse, N. Kauer, R. Blazquez, L. Hacker, S.-M. Decking, T. Bohn, S. Faerber, K. Evert, L. Aigle, S. Amslinger, M. Landa, O. Krijgsman, E. A. Rozeman, C. Brummer, P. J. Siska, K. Singer, S. Pektor, M. Miederer, K. Peter, E. Gottfried, W. Herr, I. Marchiq, J. Pouyssegur, W. R. Roush, S. Ong, S. Warren, T. Pukrop, P. Beckhove, S. A. Lang, T. Bopp, C. U. Blank, J. L. Cleveland, P. J. Oefner, K. Dettmer, M. Selby, M. Kreutz, Restricting glycolysis preserves T cell effector functions and augments checkpoint therapy. *Cell Rep.* **29**, 135–150.e9 (2019).

14. A. Calcinotto, P. Filipazzi, M. Grioni, M. Iero, A. De Milito, A. Ricupito, A. Cova, R. Canese, E. Jachetti, M. Rossetti, V. Huber, G. Parmiani, L. Generoso, M. Santinami, M. Borghi, S. Fais, M. Bellone, L. Rivoltini, Modulation of microenvironment acidity reverses anergy in human and murine tumor-infiltrating T lymphocytes. *Cancer Res.* **72**, 2746–2756 (2012).

15. Z. Husain, Y. Huang, P. Seth, V. P. Sukhatme, Tumor-derived lactate modifies antitumor immune response: Effect on myeloid-derived suppressor cells and NK cells. *J. Immunol.* **191**, 1486–1495 (2013).

16. E. Gottfried, L. A. Kunz-Schughart, S. Ebner, W. Mueller-Klieser, S. Hoves, R. Andreesen, A. Mackensen, M. Kreutz, Tumor-derived lactic acid modulates dendritic cell activation and antigen expression. *Blood* **107**, 2013–2021 (2006).

17. A. M. Levin, D. L. Bates, A. M. Ring, C. Krieg, J. T. Lin, L. Su, I. Moraga, M. E. Raeber, G. R. Bowman, P. Novick, V. S. Pande, C. G. Fathman, O. Boyman, K. C. Garcia, Exploiting a natural conformational switch to engineer an interleukin-2 superkine. *Nature* **484**, 529–533 (2012).

18. M. E. Pipkin, J. A. Sacks, F. Cruz-Guilloty, M. G. Lichtenheld, M. J. Bevan, A. Rao, Interleukin-2 and inflammation induce distinct transcriptional programs that promote the differentiation of effector cytolytic T cells. *Immunity* **32**, 79–90 (2010).

19. A. Brand, K. Singer, G. E. Koehl, M. Kolitzus, G. Schoenhammer, A. Thiel, C. Matos, C. Bruss, S. Klobuch, K. Peter, M. Kastenberger, C. Bogdan, U. Schleicher, A. Mackensen, E. Ullrich, S. Fichtner-Feigl, R. Kesselring, M. Mack, U. Ritter, M. Schmid, C. Blank, K. Dettmer, P. J. Oefner, P. Hoffmann, S. Walenta, E. K. Geissler, J. Pouyssegur, A. Villunger, A. Steven, B. Seliger, S. Schreml, S. Haferkamp, E. Kohl, S. Karrer, M. Berneburg, W. Herr, W. Mueller-Klieser, K. Renner, M. Kreutz, LDHA-associated lactic acid production blunts tumor immunosurveillance by T and NK cells. *Cell Metab.* **24**, 657–671 (2016).

20. M. D. Buck, R. T. Sowell, S. M. Kaech, E. L. Pearce, Metabolic instruction of immunity. *Cell* **169**, 570–586 (2017).

21. C.-H. Chang, J. D. Curtis, L. B. Maggi, B. Faubert, A. V. Villarino, D. O'Sullivan, S. C.-C. Huang, G. J. W. van der Windt, J. Blagih, J. Qiu, J. D. Weber, E. J. Pearce, R. G. Jones, E. L. Pearce, Posttranscriptional control of T cell effector function by aerobic glycolysis. *Cell* **153**, 1239–1251 (2013).

22. V. Huber, C. Camisaschi, A. Berzi, S. Ferro, L. Lugini, T. Triulzi, A. Tuccitto, E. Tagliabue, C. Castelli, L. Rivoltini, Cancer acidity: An ultimate frontier of tumor immune escape and a novel target of immunomodulation. *Semin. Cancer Biol.* **43**, 74–89 (2017).

23. S. Pilon-Thomas, K. N. Kodumudi, A. E. El-Kenawi, S. Russell, A. M. Weber, K. Luddy, M. Damaghi, J. W. Wojtkowiak, J. J. Mulé, A. Ibrahim-Hashim, R. J. Gillies, Neutralization of tumor acidity improves antitumor responses to immunotherapy. *Cancer Res.* **76**, 1381–1390 (2016).

24. M. A. Cox, L. E. Harrington, A. J. Zajac, Cytokines and the inception of CD8 T cell responses. *Trends Immunol.* **32**, 180–186 (2011).

25. S. Mitra, A. M. Ring, S. Amarnath, J. B. Spangler, P. Li, W. Ju, S. Fischer, J. Oh, R. Spolski, K. Weiskopf, H. Kohrt, J. E. Foley, S. Rajagopalan, E. O. Long, D. H. Fowler, T. A. Waldmann, K. C. Garcia, W. J. Leonard, Interleukin-2 activity can be fine tuned with engineered receptor signaling clamps. *Immunity* **42**, 826–838 (2015).

26. M. Sukumar, J. Liu, Y. Ji, M. Subramanian, J. G. Crompton, Z. Yu, R. Roychoudhuri, D. C. Palmer, P. Muranski, E. D. Karoly, R. P. Mohney, C. A. Klebanoff, A. Lal, T. Finkel, N. P. Restifo, L. Gattinoni, Inhibiting glycolytic metabolism enhances CD8+ T cell memory and antitumor function. *J. Clin. Invest.* **123**, 4479–4488 (2013).

27. V. Peperzak, E. A. M. Veraar, Y. Xiao, N. Bąbała, K. Thiadens, M. Brugmans, J. Borst, CD8+ T cells produce the chemokine CXCL10 in response to CD27/CD70 costimulation to promote generation of the CD8+ effector T cell pool. *J. Immunol.* **191**, 3025–3036 (2013).

28. C. Lamaze, A. Dujeancourt, T. Baba, C. G. Lo, A. Benmerah, A. Dautry-Varsat, Interleukin 2 receptors and detergent-resistant membrane domains define a Clathrin-independent endocytic pathway. *Mol. Cell* **7**, 661–671 (2001).

29. H. Wu, V. Estrella, M. Beatty, D. Abrahams, A. El-Kenawi, S. Russell, A. Ibrahim-Hashim, D. L. Longo, Y. K. Reshetnyak, A. Moshnikova, O. A. Andreev, K. Luddy, M. Damaghi, K. Kodumudi, S. R. Pillai, P. Enriquez-Navas, P. Pilon-Thomas, P. Swietach, R. J. Gillies, T-cells produce acidic niches in lymph nodes to suppress their own effector functions. *Nat. Commun.* **11**, 4113 (2020).

30. S. A. Rosenberg, J. C. Yang, D. E. White, S. M. Steinberg, Durability of complete responses in patients with metastatic cancer treated with high-dose interleukin-2: Identification of the antigens mediating response. *Ann. Surg.* **228**, 307–319 (1998).

31. S. A. Feldman, Y. Assadipour, I. Kriley, S. L. Goff, S. A. Rosenberg, Adoptive cell therapy-- tumor-infiltrating lymphocytes, T-cell receptors, and chimeric antigen receptors. *Semin. Oncol.* **42**, 626–639 (2015).

32. S. Türkcan, L. Kiru, D. J. Naczynski, L. S. Sasportas, G. Pratx, Lactic acid accumulation in the tumor microenvironment suppresses ^{18}F-FDG uptake. *Cancer Res.* **79**, 410–419 (2019).

33. B. P. Nicolet, A. Guislain, F. P. J. van Alphen, R. Gomez-Eerland, T. N. M. Schumacher, M. van den Biggelaar, M. C. Wolkers, CD29 identifies IFN-γ-producing human CD8+ T cells with an increased cytotoxic potential. *Proc. Natl. Acad. Sci. U.S.A.* **117**, 6686–6696 (2020).

34. Z. Zhou, H. He, K. Wang, X. Shi, Y. Wang, Y. Su, Y. Wang, D. Li, W. Liu, Y. Zhang, L. Shen, W. Han, L. Shen, J. Ding, F. Shao, Granzyme A from cytotoxic lymphocytes cleaves GSDMB to trigger pyroptosis in target cells. *Science* **368**, eaaz7548 (2020).

35. A. Brewitz, S. Eickhoff, S. Dähling, T. Quast, S. Bedoui, R. A. Kroczek, C. Kurts, N. Garbi, W. Barchet, M. Iannacone, F. Klauschen, W. Kolanus, T. Kaisho, M. Colonna, R. N. Germain, W. Kastenmüller, CD8+ T cells orchestrate pDC-XCR1+ dendritic cell spatial and functional cooperativity to optimize Priming. *Immunity* **46**, 205–219 (2017).

36. C. Krieg, S. Létourneau, G. Pantaleo, O. Boyman, Improved IL-2 immunotherapy by selective stimulation of IL-2 receptors on lymphocytes and endothelial cells. *Proc. Natl. Acad. Sci. U.S.A.* **107**, 11906–11911 (2010).

37. D. J. Peace, M. A. Cheever, Toxicity and therapeutic efficacy of high-dose interleukin 2. In vivo infusion of antibody to NK-1.1 attenuates toxicity without compromising efficacy against murine leukemia. *J. Exp. Med.* **169**, 161–173 (1989).

38. I. Vanni, E. Ugolotti, A. Raso, E. D. Marco, R. Melioli, R. Biassoni, Development and validation of a multiplex quantitative polymerase chain reaction assay for the detection of Mollicutes impurities in human cells, cultured under good manufacturing practice conditions, and following European Pharmacopoeia requirements and the International Conference on Harmonization guidelines. *Cytotherapy* **14**, 752–766 (2012).

39. X. Wang, M. Rickert, K. C. Garcia, Structure of the quaternary complex of Interleukin-2 with Its α, ß, and γc receptors. *Science* **310**, 1159–1163 (2005).

40. J. Yin, P. D. Straight, S. M. McLoughlin, Z. Zhou, A. J. Lin, D. E. Golan, N. L. Kelleher, R. Kolter, C. T. Walsh, Genetically encoded short peptide tag for versatile protein labeling by Sfp phosphopantetheinyl transferase. *Proc. Natl. Acad. Sci. U.S.A.* **102**, 15815–15820 (2005).

41. S. Wilmes, O. Beutel, Z. Li, V. Francois-Newton, C. P. Richter, D. Janning, C. Kroll, P. Hanhart, K. Hötte, C. You, G. Uzé, S. Pellegrini, J. Piehler, Receptor dimerization dynamics as a regulatory valve for plasticity of type I interferon signaling. *J. Cell Biol.* **209**, 579–593 (2015).

42. P. O. Krutzik, G. P. Nolan, Fluorescent cell barcoding in flow cytometry allows high-throughput drug screening and signaling profiling. *Nat. Methods* **3**, 361–368 (2006).

43. E. T. Boder, K. D. Wittrup, Yeast surface display for screening combinatorial polypeptide libraries. *Nat. Biotechnol.* **15**, 553–557 (1997).

44. G. Winter, D. G. Waterman, J. M. Parkhurst, A. S. Brewster, R. J. Gildea, M. Gerstel, L. Fuentes-Montero, M. Vollmar, T. Michels-Clark, I. D. Young, N. K. Sauter, G. Evans, DIALS: Implementation and evaluation of a new integration package. *Acta Crystallogr. Sect. Struct. Biol.* **74**, 85–97 (2018).

45. P. R. Evans, G. N. Murshudov, How good are my data and what is the resolution? *Acta Crystallogr. D Biol. Crystallogr.* **69**, 1204–1214 (2013).

46. M. D. Winn, C. C. Ballard, K. D. Cowtan, E. J. Dodson, P. Emsley, P. R. Evans, R. M. Keegan, E. B. Krissinel, A. G. W. Leslie, A. McCoy, S. J. McNicholas, G. N. Murshudov, N. S. Pannu, E. A. Potterton, H. R. Powell, R. J. Read, A. Vagin, K. S. Wilson, Overview of the *CCP4* suite and current developments. *Acta Crystallogr. D Biol. Crystallogr.* **67**, 235–242 (2011).

47. A. J. McCoy, R. W. Grosse-Kunstleve, P. D. Adams, M. D. Winn, L. C. Storoni, R. J. Read, Phaser crystallographic software. *J. Appl. Cryst.* **40**, 658–674 (2007).

48. D. Liebschner, P. V. Afonine, M. L. Baker, G. Bunkóczi, V. B. Chen, T. I. Croll, B. Hintze, L. W. Hung, S. Jain, A. J. McCoy, N. W. Moriarty, R. D. Oeffner, B. K. Poon, M. G. Prisant, R. J. Read, J. S. Richardson, D. C. Richardson, M. D. Sammito, O. V. Sobolev, D. H. Stockwell, T. C. Terwilliger, A. G. Urzhumtsev, L. L. Videau, C. J. Williams, P. D. Adams, Macromolecular structure determination using X-rays, neutrons and electrons: Recent developments in Phenix. *Acta Crystallogr. Sect. Struct. Biol.* **75**, 861–877 (2019).

49. P. Emsley, K. Cowtan, Coot: Model-building tools for molecular graphics. *Acta Crystallogr. D Biol. Crystallogr.* **60**, 2126–2132 (2004).

50. V. B. Chen, W. B. Arendall, J. J. Headd, D. A. Keedy, R. M. Immormino, G. J. Kapral, L. W. Murray, J. S. Richardson, D. C. Richardson, MolProbity: All-atom structure validation for macromolecular crystallography. *Acta Crystallogr. D Biol. Crystallogr.* **66**, 12–21 (2010).

51. M. I. Love, W. Huber, S. Anders, Moderated estimation of fold change and dispersion for RNA-seq data with DESeq2. *Genome Biol.* **15**, 550 (2014).

52. G. Yu, L.-G. Wang, Y. Han, Q.-Y. He, clusterProfiler: An R package for comparing biological themes among gene clusters. *OMICS* **16**, 284–287 (2012).

53. G. X. Y. Zheng, J. M. Terry, P. Belgrader, P. Ryvkin, Z. W. Bent, R. Wilson, S. B. Ziraldo, T. D. Wheeler, G. P. McDermott, J. Zhu, M. T. Gregory, J. Shuga, L. Montesclaros, J. G. Underwood, D. A. Masquelier, S. Y. Nishimura, M. Schnall-Levin, P. W. Wyatt, C. M. Hindson, R. Bharadwaj, A. Wong, K. D. Ness, L. W. Beppu, H. J. Deeg, C. McFarland, K. R. Loeb, W. J. Valente, N. G. Ericson, E. A. Stevens, J. P. Radich, T. S. Mikkelsen, B. J. Hindson, J. H. Bielas, Massively parallel digital transcriptional profiling of single cells. *Nat. Commun.* **8**, 14049 (2017).

54. Y. Hao, S. Hao, E. Andersen-Nissen, W. M. Mauck, S. Zheng, A. Butler, M. J. Lee, A. J. Wilk, C. Darby, M. Zager, P. Hoffman, M. Stoeckius, E. Papalexi, E. P. Mimitou, J. Jain, A. Srivastava, T. Stuart, L. M. Fleming, B. Yeung, A. J. Rogers, J. M. McElrath, C. A. Blish, R. Gottardo, P. Smibert, R. Satija, Integrated analysis of multimodal single-cell data. *Cell* **184**, 3573–3587.e29 (2021).

55. C. You, C. P. Richter, S. Löchte, S. Wilmes, J. Piehler, Dynamic submicroscopic signaling zones revealed by pair correlation tracking and localization microscopy. *Anal. Chem.* **86**, 8593–8602 (2014).

56. I. Moraga, G. Wernig, S. Wilmes, V. Gryshkova, C. P. Richter, W.-J. Hong, R. Sinha, F. Guo, H. Fabionar, T. S. Wehrman, P. Krutzik, S. Demharter, I. Plo, I. L. Weissman, P. Minary, R. Majeti, S. N. Constantinescu, J. Piehler, K. C. Garcia, Tuning cytokine receptor signaling by re-orienting dimer geometry with surrogate ligands. *Cell* **160**, 1196–1208 (2015).

57. J. Vogelsang, R. Kasper, C. Steinhauer, B. Person, M. Heilemann, M. Sauer, P. Tinnefeld, A reducing and oxidizing system minimizes photobleaching and blinking of fluorescent dyes. *Angew. Chem. Int. Ed. Engl.* **47**, 5465–5469 (2008).

58. A. Sergé, N. Bertaux, H. Rigneault, D. Marguet, Dynamic multiple-target tracing to probe spatiotemporal cartography of cell membranes. *Nat. Methods* **5**, 687–694 (2008).

59. A. Šali, T. L. Blundell, Comparative protein modelling by satisfaction of spatial restraints. *J. Mol. Biol.* **234**, 779–815 (1993).

60. M. H. M. Olsson, C. R. Søndergaard, M. Rostkowski, J. H. Jensen, PROPKA3: Consistent treatment of internal and surface residues in empirical p*K*a predictions. *J. Chem. Theory Comput.* **7**, 525–537 (2011).

61. S. Piana, P. Robustelli, D. Tan, S. Chen, D. E. Shaw, Development of a force field for the simulation of single-chain proteins and protein–protein complexes. *J. Chem. Theory Comput.* **16**, 2494–2507 (2020).

62. S. Piana, A. G. Donchev, P. Robustelli, D. E. Shaw, Water dispersion interactions strongly influence simulated structural properties of disordered protein states. *J. Phys. Chem. B* **119**, 5113–5123 (2015).

63. M. J. Abraham, T. Murtola, R. Schulz, S. Páll, J. C. Smith, B. Hess, E. Lindahl, GROMACS: High performance molecular simulations through multi-level parallelism from laptops to supercomputers. *SoftwareX* **1–2**, 19–25 (2015).

64. G. Bussi, D. Donadio, M. Parrinello, Canonical sampling through velocity rescaling. *J. Chem. Phys.* **126**, 014101 (2007).

65. M. Parrinello, A. Rahman, Polymorphic transitions in single crystals: A new molecular dynamics method. *J. Appl. Phys.* **52**, 7182–7190 (1981).

66. R. T. McGibbon, K. A. Beauchamp, M. P. Harrigan, C. Klein, J. M. Swails, C. X. Hernández, C. R. Schwantes, L.-P. Wang, T. J. Lane, V. S. Pande, MDTraj: A modern open library for the analysis of molecular dynamics trajectories. *Biophys. J.* **109**, 1528–1532 (2015).

IL-2 is inactivated by the acidic pH environment of tumors enabling engineering of a pH-selective mutein

Silvia Gaggero, Jonathan Martinez-Fabregas, Adeline Cozzani, Paul K. Fyfe, Malo Leprohon, Jie Yang, F. Emil Thomasen, Hauke Winkelmann, Romain Magnez, Alberto G. Conti, Stephan Wilmes, Elizabeth Pohler, Manuel van Gijsel Bonnello, Xavier Thuru, Bruno Quesnel, Fabrice Soncin, Jacob Piehler, Kresten Lindorff-Larsen, Rahul Roychoudhuri, Ignacio Moraga, and Suman Mitra

Acid-tolerant IL-2 targets tumors
Hypoxic and acidic conditions prevalent in the tumor microenvironment present a formidable challenge for host lymphocytes trying to eradicate cancer cells. IL-2, a cytokine supporting CD8 T cell and NK cell functions, exhibits markedly compromised binding to the IL-2R# receptor chain at pH 6 and below. Gaggero *et al.* used directed evolution to screen for IL-2 variants with mutations at the receptor interface that enhanced receptor binding at low pH. A mutated "Switch-2" variant of IL-2 with strong receptor binding at pH 6 but minimal interaction at neutral pH exhibited enhanced in vivo antitumor activity in mice. Recognition of the pH sensitivity of IL-2 and other cytokines will spur engineering of cytokine variants capable of enhanced performance in the acidic tumor microenvironment.

View the article online
https://www.science.org/doi/10.1126/sciimmunol.ade5686
Permissions
https://www.science.org/help/reprints-and-permissions

Use of this article is subject to the Terms of service